UILU-ENG-85-2003

CIVIL ENGINEERING STUDIES

STRUCTURAL RESEARCH SERIES NO. 518

ISSN: 0069-4274

STRESS INTERFERENCE IN AXISYMMETRIC TORSION OF A TRANSVERSELY ISOTROPIC BODY

By
S. M. HEINRICH
and
R. A. EUBANKS

Technical Report of Research
Sponsored by
THE AIR FORCE OFFICE OF SCIENTIFIC RESEARCH
(Grant No. AFOSR 82-0047)

UNIVERSITY OF ILLINOIS
at URBANA-CHAMPAIGN
URBANA, ILLINOIS
MAY 1985

STRESS INTERFERENCE IN AXISYMMETRIC TORSION OF A TRANSVERSELY ISOTROPIC BODY

by

S. M. HEINRICH

and

R. A. EUBANKS

A Technical Report of
Research Sponsored by

THE AIR FORCE OFFICE
OF SCIENTIFIC RESEARCH
Grant No. AFOSR 82-0047

University of Illinois
at Urbana-Champaign
Urbana, Illinois

May 1985

50272-101

REPORT DOCUMENTATION PAGE	1. REPORT NO. UILU-ENG-85-2003	2.	3. Recipient's Accession No.

4. Title and Subtitle
Stress Interference in Axisymmetric Torsion of a Transversely Isotropic Body

5. Report Date
Published May 1985

6.

7. Author(s)
S. M. Heinrich and R. A. Eubanks

8. Performing Organization Rept. No.
SRS No. 518

9. Performing Organization Name and Address
Department of Civil Engineering
University of Illinois
208 N. Romine St.
Urbana, Illinois 61801

10. Project/Task/Work Unit No.
2307/B1

11. Contract(C) or Grant(G) No.
(C)
(G) AFOSR 82-0047

12. Sponsoring Organization Name and Address
Air Force Office of Scientific Research
Structural Mechanics Division
Bolling Air Force Base
Washington, D.C. 20332

13. Type of Report & Period Covered
Technical Report

14.

15. Supplementary Notes

16. Abstract (Limit: 200 words)

An unbounded transversely isotropic body of revolution containing two spheroidal cavities is subjected to torsion about its axis of elastic symmetry, which coincides with its axis of revolution. At large distances from the cavities the elastic field approaches the Saint-Venant solution for the torsion of a circular cylinder. The elasticity solution is obtained in series form and numerical results presented for the case of two spherical cavities. Of primary interest is the degree of stress interference between the two perturbations, as a function of the spacing of the cavities and the values of the elastic constants.

17. Document Analysis a. Descriptors

Anisotropy
Fiber-Reinforced Composites
Stress Concentration
Stress Function
Stress Interference
Three-Dimensional Linear Elasticity
Torsion
Transverse Isotropy

b. Identifiers/Open-Ended Terms

c. COSATI Field/Group

18. Availability Statement	19. Security Class (This Report)	21. No. of Pages
Approved for public release -- Distribution unlimited	UNCLASSIFIED	96
	20. Security Class (This Page) UNCLASSIFIED	22. Price

(See ANSI-Z39.18) *See Instructions on Reverse* OPTIONAL FORM 272 (4-77) (Formerly NTIS-35) Department of Commerce

ACKNOWLEDGMENTS

This report was prepared as a doctoral dissertation by Mr. Stephen Michael Heinrich and was submitted to the Graduate College of the University of Illinois at Urbana-Champaign in partial fulfillment of the requirements for the degree of Doctor of Philosophy in Civil Engineering. The investigation was performed under the supervision of Dr. R. A. Eubanks, Professor of Civil Engineering and of Theoretical and Applied Mechanics.

The study was conducted as part of a research program sponsored by the Air Force Office of Scientific Research under Grant No. AFOSR 82-0047. This financial support is gratefully acknowledged.

The numerical results presented herein were obtained using the CDC Cyber 175 computer system of the Computing Services Office of the University of Illinois.

TABLE OF CONTENTS

Page

LIST OF TABLES

LIST OF SYMBOLS

a	length of semi-axis of spheroidal cavities along r-direction; also, scaling factor for non-dimensionalizing coordinates and displacement field
$a_m^{(n)}$, $\bar{a}_m^{(n)}$	Legendre coefficients
A_n, $\bar{A}_n$	coefficients of superposition for ψ , n = 2, 3, ...
$A_n^{(N)}$,$\bar{A}_n^{(N)}$	coefficients of superposition for $\psi^{(N)}$, n = 2, 3, ..., N
c_{44}	shear modulus in the r-z plane
c_{66}	shear modulus in the r-θ plane
n_j	cosine of the angle between the j-axis and the unit outward normal $\underset{\sim}{n}$ at a point on a surface
(p_1,q_1,θ)	spheroidal coordinates centered at the upper cavity, orthogonal in the (r, θ, z_3)-space
(p_2,q_2,θ)	spheroidal coordinates centered at the lower cavity, orthogonal in the (r, θ, z_3)-space
(p,q,θ)	spheroidal coordinates centered at upper cavity, orthogonal in the "physical" (r, θ, z)-space
$\hat{p}_2(p_1,q_1),\hat{q}_2(p_1,q_1)$	functions relating (p_1,q_1) to (p_2,q_2)
$\hat{\bar{p}}_2(p_1,\hat{\bar{q}}_1),\hat{\bar{q}}_2(p_1,\hat{\bar{q}}_1)$	functions relating $(p_1,\bar{q}_1)$ to $(p_2,\bar{q}_2)$ for $\kappa_3 < 1$
$P_n(p)$	Legendre polynomial of degree n
$P_n^2(p)$, $Q_n^2(q)$	associated Legendre functions of degree n and order 2, of the first and second kinds, respectively
$\bar{Q}_n^2(\bar{q})$	$= \dfrac{Q_n^2(q)}{i^{n+1}}$ for $\kappa_3 < 1$

q_0 — $= \frac{\kappa_3}{\alpha}$, value of q_1 and q_2 on upper and lower cavity surfaces, respectively

$\bar{q}_j$ — $= -i\, q_j$ for $\kappa_3 < 1$, $j = 0,1,2$

(r,θ,z) — non-dimensionalized circular cylindrical coordinates

s — non-dimensionalized arc length parameter along C_i and C_o

s_3 — non-dimensionalized arc length parameter along C_i' and C_o'

SCF — $= \left. \frac{\sigma_{p\theta}^{(N)}}{\sigma_{p\theta}^{(0)}} \right|_{q_1=q_0}$, stress concentration factor

SIF — $= \left(\frac{\sigma_{p\theta}\big|_{\lambda\to\bar{\infty}} - \sigma_{p\theta}}{\sigma_{p\theta}\big|_{\lambda\to\infty}} \right)\Bigg|_{q_1=q_0} \times 100\%$, stress interference factor (percent interference)

T_θ — tangential traction component prescribed on cavity surfaces

$T_\theta^{(N)}$ — tangential traction component on cavity surfaces generated by $\psi^{(N)}$

$T_\theta^{(0)}$ — tangential traction component on cavity surfaces due to ψ_0

$\delta u_i^{(n)}$ — components of virtual displacement field

u_r, u_θ, u_z — non-dimensionalized components of the displacement field

z_3 — $= \frac{z}{\nu_3}$

$\mathcal{B}$ — region occupied by the transversely isotropic body of revolution

C_i, C_o — generating curves for S_i and S_o, respectively; also, lateral boundaries of $\mathcal{R}$

$\mathcal{R}$ — planar region consisting of one half of a meridional section of $\mathcal{B}$

S_i, S_o — inner and outer lateral surfaces bounding $\mathcal{B}$, respectively

$\mathcal{B}'$, C_i', C_o', $\mathcal{R}'$ — maps of $\mathcal{B}$, C_i, C_o, and $\mathcal{R}$ in the (r, θ, z_3)-space, respectively

$$\alpha = \begin{cases} \sqrt{\kappa_3^2 - 1} & , \ \kappa_3 > 1 \\ -i\sqrt{1 - \kappa_3^2} & , \ \kappa_3 < 1 \end{cases}$$

$$\bar{\alpha} = i\alpha$$

$$\alpha_0 = \begin{cases} \sqrt{\kappa^2 - 1} & , \ \kappa > 1 \\ -i\sqrt{1 - \kappa^2} & , \ \kappa < 1 \end{cases}$$

$$\beta = \frac{2\lambda_3}{\alpha}$$

$$\bar{\beta} = -i\beta$$

$$\delta_{m,n} = \begin{cases} 1 & , \ m = n \\ 0 & , \ m \neq n \end{cases}$$ (Kronecker delta)

$$\varepsilon(N; \lambda, \nu_3) = \lim_{p \to -1} \left| \frac{T_\theta^{(N)}(p)}{T_\theta^{(0)}(p)} \right|$$, relative residual traction at inner pole of cavity

ε_{rr}, $\varepsilon_{\theta\theta}$, ... , $\gamma_{r\theta}$ — circular cylindrical components of infinitesimal engineering strain

κ	aspect ratio of spheroidal cavities $\left(\frac{\text{z semi-axis}}{\text{r semi-axis}}\right)$
κ_3	$= \frac{\kappa}{\nu_3}$
λ	spacing parameter of twin cavities, whose centers are separated by a distance $2\lambda a$
λ_3	$= \frac{\lambda}{\nu_3}$
ν_3	$= \left(\frac{c_{44}}{c_{66}}\right)^{\frac{1}{2}}$
ω	$= \frac{u_\theta}{r}$, angle of twist
ψ	stress function
$\psi^{(N)}$	approximate stress function, $N \geq 2$
ψ_0	stress function corresponding to uniform torsion
σ_{ij}	components of stress
$\sigma_{ij}^{(N)}$	approximate stress field generated by $\psi^{(N)}$
$\sigma_{ij}^{(0)}$	components of the uniform (non-perturbed) stress field
τ	angle of twist per unit length corresponding to uniform torsion field
Θ	angle defined in Fig. 5.3.1; running variable on cavity surfaces

CHAPTER 1

INTRODUCTION

1.1 Objective and Scope

Three-dimensional boundary value problems in anisotropic elasticity theory are inherently more complex than their isotropic counterparts, due to the presence of more than two elastic constants in the generalized Hooke's law. Despite this added complexity, a large number of technically significant problems have been solved for the case of transverse isotropy, a type of anisotropy characterized by five elastic constants. While some of these solutions demonstrate the phenomenon of stress concentration, in which a uniform stress field in an infinite body is disturbed by a single cavity or inclusion [2-9], it appears that the problem of "stress interference", or the interaction between multiple perturbing stress fields, in an anisotropic medium has not been addressed in the literature. The phenomenon of stress interference in isotropic materials has received considerable attention (see survey article by Sternberg [39]).

In the present work, a solution is given for the problem of the torsion of a transversely isotropic body of revolution containing two spheroidal cavities. The objective of the investigation is twofold:

1) The solution presented will demonstrate the phenomenon of stress interference, and the closely related Principle of Saint-Venant, in a three-dimensional anisotropic elasticity problem;

2) The method utilized in obtaining the solution of the torsion problem may be extended to include other loading cases (tension, shear, flexure), other boundary conditions (elastic inclusion), or the case in which the body contains more than two cavities.

1.2 History of Stress Interference Problems

Stress interference is the interaction between perturbing stress fields, due to two or more sources of stress concentration in an elastic solid. The stress concentrations may be caused by geometric or material discontinuities. The problem of stress interference arises in the interpretation of non-destructive test results for welds, forgings, and castings, which show the sizes and locations of material flaws [15]. Considerations of this type become critical in the design and quality control of pressure vessels and rocket cases, as well as other types of structures [35]. Several problems have been solved which illustrate the phenomenon of stress interference in a three-dimensional isotropic elastic solid. Those results related to interference caused by the presence of multiple cavities or inclusions in the body are surveyed below.

In 1952 Sternberg and Sadowsky [40] solved the problem of two spherical cavities in an infinite isotropic elastic solid under axisymmetric loading on the cavity surfaces and homogeneous tractions at infinity. They developed and employed spherical dipolar harmonics to obtain the solution. Shelley and Yu [38] used a similar approach to consider the interference between two rigid spherical inclusions when the stress field at infinity is uniaxial or hydrostatic tension. In a discussion of [38], Hill [19]

presented results for the uniaxial case in which the rigid inclusions are of unequal diameter. Eubanks [12] appears to have been the first to attack the stress interference problem for axisymmetric torsion when he considered the torsion of an infinite isotropic elastic body containing two spherical cavities. He obtained the solution in the form of an explicit series. Hill [20] extended the work to the case in which the infinite solid is bonded to two rigid spherical inclusions, while Goree and Wilson [14] investigated the effect of partially bonded rigid inclusions, upon which non-vanishing resultant torques may act. Problems of stress interference due to an infinite row of spherical or spheroidal cavities were solved by Miyamoto [32], Atsumi [1], and Nisitani [34]. In each case the loading considered was uniaxial tension along the line of cavities. Atsumi did not restrict his investigation to "small" cavities, as he considered the cavities to lie on the centerline of a cylinder of finite radius.

While all these solutions are for isotropic bodies, no multiple cavity or multiple inclusion problem is known to have been solved for an anisotropic solid. In the present study a solution is given for the torsion problem for an infinite anisotropic elastic body containing two spheroidal cavities. The particular type of anisotropy considered is that for which the Hookean matrix remains invariant under an arbitrary rotation of the coordinate system about an axis (the "axis of elastic symmetry" of the material). A material of this type is called "transversely isotropic."

1.3 Transverse Isotropy

For a transversely isotropic material, with z-axis the axis of elastic symmetry, the generalized Hooke's law in circular cylindrical coordinates takes the form [13]

$$\begin{Bmatrix} \sigma_{rr} \\ \sigma_{\theta\theta} \\ \sigma_{zz} \\ \sigma_{\theta z} \\ \sigma_{rz} \\ \sigma_{r\theta} \end{Bmatrix} = \begin{bmatrix} c_{11} & c_{12} & c_{13} & 0 & 0 & 0 \\ c_{12} & c_{11} & c_{13} & 0 & 0 & 0 \\ c_{13} & c_{13} & c_{33} & 0 & 0 & 0 \\ 0 & 0 & 0 & c_{44} & 0 & 0 \\ 0 & 0 & 0 & 0 & c_{44} & 0 \\ 0 & 0 & 0 & 0 & 0 & c_{66} \end{bmatrix} \begin{Bmatrix} \varepsilon_{rr} \\ \varepsilon_{\theta\theta} \\ \varepsilon_{zz} \\ \gamma_{\theta z} \\ \gamma_{rz} \\ \gamma_{r\theta} \end{Bmatrix}, \qquad (1.3.1)$$

where

$$c_{66} = \frac{1}{2}(c_{11} - c_{12}) \qquad (1.3.2)$$

and

$\varepsilon_{rr}, \varepsilon_{\theta\theta}, \ldots$ are the components of infinitesimal engineering strain defined by

$$\left.\begin{aligned}
\varepsilon_{rr} &= \frac{\partial u_r}{\partial r} \quad , \\
\varepsilon_{\theta\theta} &= \frac{1}{r}\frac{\partial u_\theta}{\partial \theta} + \frac{u_r}{r} \quad , \\
\varepsilon_{zz} &= \frac{\partial u_z}{\partial z} \quad , \\
\gamma_{\theta z} &= \frac{\partial u_\theta}{\partial z} + \frac{1}{r}\frac{\partial u_z}{\partial \theta} \quad , \\
\gamma_{rz} &= \frac{\partial u_z}{\partial r} + \frac{\partial u_r}{\partial z} \quad , \\
\gamma_{r\theta} &= \frac{1}{r}\frac{\partial u_r}{\partial \theta} + \frac{\partial u_\theta}{\partial r} - \frac{u_\theta}{r} \quad ,
\end{aligned}\right\} \tag{1.3.3}$$

where u_r, u_θ, u_z are the components of the displacement vector.

Necessary and sufficient conditions for the positive definiteness of the strain energy function are the following [13]:

$$\begin{aligned}
&c_{11} > 0 \quad , \quad c_{33} > 0 \quad , \quad c_{44} > 0 \quad , \quad c_{66} > 0 \quad , \\
&c_{11}c_{33} - c_{13}^2 - c_{33}c_{66} > 0 \quad .
\end{aligned} \tag{1.3.4}$$

A material obeying the constitutive relation (1.3.1) will demonstrate elastic symmetry in planes perpendicular to the z-axis; i.e., all directions in the r-θ plane are elastically equivalent. For this reason planes parallel to the r-θ plane are sometimes referred to as "planes of isotropy". Some materials exhibiting transversely isotropic behavior are wood, stratified soil or rock, and materials possessing an hexagonal

crystalline structure, such as magnesium, cadmium, and zinc. Graphite is highly transversely isotropic, as are unidirectional fiber-reinforced composites [17,29]. Some typical values of the elastic constants for a few of these materials are listed in Table 1.1 [25,29], in which $\nu_3 \equiv \left(\frac{c_{44}}{c_{66}}\right)^{\frac{1}{2}}$ is the elastic parameter which arises in torsion problems.

Table 1.1 Elastic Constants for Some Transversely Isotropic Materials

Material	c_{11}	c_{33}	c_{44}	c_{12}	c_{13}	ν_3
Cadmium	110 GPa	46.9 GPa	15.6 GPa	40.4 GPa	38.3 GPa	.670
Zinc	161	61.0	38.3	34.2	50.1	.777
Magnesium	59.7	61.7	16.4	26.2	21.7	.989
Modmor II Graphite Fibers	20.0	237	24.0	9.94	8.37	2.18
Modmor II/LY558 Graphite-Epoxy Composite (0.67 Fiber-Volume Fraction)	14.5	161	7.10	7.21	6.50	1.40

1.4 Organization of the Study

The general stress function approach for the torsion of transversely isotropic bodies of revolution is derived in Chapter 2. The results are extended to the case in which the body is unbounded.

In Chapter 3 the general results of Chapter 2 are applied to the specific problem of the torsion of an infinite transversely isotropic body of revolution containing two spheroidal cavities, thus resulting in a corresponding Dirichlet boundary value problem for the stress function.

The introduction of two spheroidal coordinate systems facilitates the mathematical description of the problem.

The method of solution used to obtain the stress function is presented in Chapter 4. After reducing the problem to an infinite system of linear algebraic equations, various interpretations of the truncated solution are discussed. Expressions are given in series form for the stresses, the stress concentration factor, and the stress interference factor. A line integral representation for the displacement is also presented.

Numerical results, which include plots of the stress concentration factor and stress interference factor along the surfaces of two spherical cavities, are presented in Chapter 5. The results are then discussed, with particular emphasis on the effect of anisotropy on the stress interference and the implications this has regarding the applicability of Saint-Venant's principle in a three-dimensional anisotropic elasticity problem.

In Chapter 6 the results of the study are summarized and recommendations for further study are made.

CHAPTER 2

TORSION OF A TRANSVERSELY ISOTROPIC BODY OF REVOLUTION - GENERAL THEORY

2.1 General

The Lekhnitskii stress function approach [31], which is an extension of the Michell-Föppl theory [37,41] for the torsion of isotropic bodies of revolution, is derived in the present chapter. This approach guarantees the existence of a stress function which generates the stress field in a transversely isotropic body of revolution subjected to axisymmetric torsion in the absence of body forces. The stress function must satisfy a second-order linear partial differential equation in the interior of the body, and meet boundary conditions of the Dirichlet type on the bounding surface(s). At the end of the chapter the approach is extended to include bodies occupying an unbounded region.

2.2 Stress Function Approach

Let (r, θ, z) denote the circular cylindrical coordinates of a point, where r and z are dimensionless quantities referring to a scale length a. Consider a transversely isotropic body of revolution occupying the region $\mathcal{B}$, whose axis of elastic symmetry coincides with its axis of revolution, the z-axis. (See Fig. 2.2.1.) Furthermore it is assumed that any transverse section of the body is bounded by at most two concentric circles, thus eliminating the possibility of toroidal (ring-like) cavities. (The derivation which follows may be modified to include this more general geometry.) For definiteness let one end of the body be rigidly fixed,

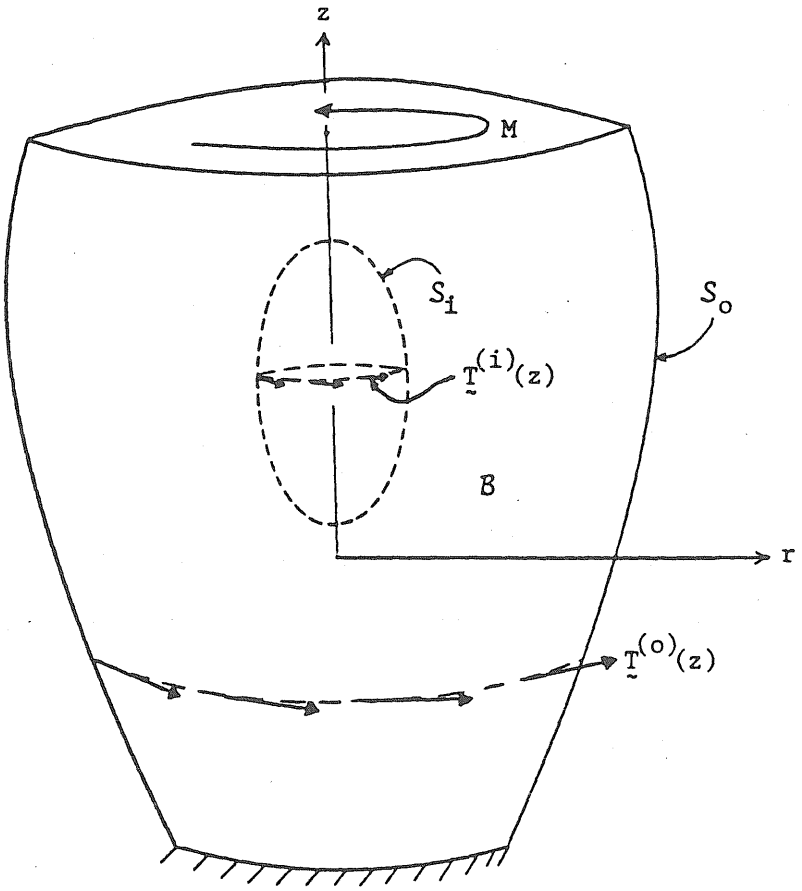

Fig. 2.2.1 Torsion of Body of Revolution

while the other is subjected to tangential tractions statically equivalent to a torque. The inner and outer lateral surfaces, S_i and S_o, are acted upon by tangential tractions $\underset{\sim}{T}^{(i)}(z) = T_\theta^{(i)}(z)\underset{\sim}{e}_\theta$ and $\underset{\sim}{T}^{(o)}(z) = T_\theta^{(o)}(z)\underset{\sim}{e}_\theta$, respectively. (Here $\underset{\sim}{e}_\theta$ is the unit base vector in the θ-direction at the point of interest.) In addition all body forces are assumed to vanish.

The derivation begins with the same underlying assumptions made in the Michell-Föppl theory; namely, that the cross sections do not warp and that no radial displacements occur:

$$u_r = u_z = 0 \ ,$$
$$u_\theta = u_\theta(r,z) \ .$$

(For convenience u_θ is also dimensionless, scaled by the length unit a.) By definition, the above displacement field characterizes a state of axisymmetric torsion. The corresponding components of engineering strain are given by

$$\left.\begin{aligned} \varepsilon_{rr} &= \varepsilon_{\theta\theta} = \varepsilon_{zz} = \gamma_{rz} = 0 \ , \\ \gamma_{r\theta} &= \frac{\partial u_\theta}{\partial r} - \frac{u_\theta}{r} \ , \\ \gamma_{\theta z} &= \frac{\partial u_\theta}{\partial z} \ , \end{aligned}\right\} \qquad (2.2.1)$$

while the stress components take the form

$$\left.\begin{aligned} &\sigma_{rr} = \sigma_{\theta\theta} = \sigma_{zz} = \sigma_{rz} = 0 \quad , \\ &\sigma_{r\theta} = c_{66}\,\gamma_{r\theta} = c_{66}\left(\frac{\partial u_\theta}{\partial r} - \frac{u_\theta}{r}\right) = c_{66}\, r \frac{\partial}{\partial r}\left(\frac{u_\theta}{r}\right) , \\ &\sigma_{\theta z} = c_{44}\,\gamma_{\theta z} = c_{44}\frac{\partial u_\theta}{\partial z} = c_{44}\, r \frac{\partial}{\partial z}\left(\frac{u_\theta}{r}\right) . \end{aligned}\right\} \qquad (2.2.2)$$

Two of the three equations of equilibrium are satisfied identically, while the third equation is the following:

$$\frac{\partial \sigma_{r\theta}}{\partial r} + \frac{\partial \sigma_{\theta z}}{\partial z} + \frac{2\sigma_{r\theta}}{r} = 0 \ ,$$

or

$$\frac{\partial}{\partial r}\left(r^2 \sigma_{r\theta}\right) + \frac{\partial}{\partial z}\left(r^2 \sigma_{\theta z}\right) = 0 \ . \qquad (2.2.3)$$

Equation (2.2.3) implies that there exists a function $\psi(r,z)$ defined in $\mathcal{B}$ such that

$$\frac{\partial \psi}{\partial z} = -\frac{\nu_3}{c_{44}}\, r^2\, \sigma_{r\theta} \ ,$$

$$\frac{\partial \psi}{\partial r} = \frac{\nu_3}{c_{44}}\, r^2\, \sigma_{\theta z} \ ,$$

or

$$\sigma_{r\theta} = -\frac{c_{44}}{\nu_3}\frac{1}{r^2}\frac{\partial\psi}{\partial z} \quad ,$$

$$\sigma_{\theta z} = \frac{c_{44}}{\nu_3}\frac{1}{r^2}\frac{\partial\psi}{\partial r} \quad , \tag{2.2.4}$$

where

$$\nu_3 \equiv \left(\frac{c_{44}}{c_{66}}\right)^{1/2} \quad . \tag{2.2.5}$$

Representation (2.2.4) ensures that the stress equation of equilibrium (2.2.3) is satisfied identically.

From equations (2.2.2) and (2.2.4) one may obtain the differential relationship between the "stress function" ψ and the angle of twist $\frac{u_\theta}{r}$:

$$\frac{\partial\psi}{\partial r} = \nu_3 r^3 \frac{\partial}{\partial z}\left(\frac{u_\theta}{r}\right) \quad ,$$

$$\frac{\partial\psi}{\partial z} = -\frac{1}{\nu_3} r^3 \frac{\partial}{\partial r}\left(\frac{u_\theta}{r}\right) \quad . \tag{2.2.6}$$

These equations imply a line integral representation for the angle of twist, while the angle of twist per unit length, $\frac{\partial}{\partial z}\left(\frac{u_\theta}{r}\right)$, may be obtained directly from the first of equations (2.2.6). Also, note that the stress function is dimensionless.

Eliminating $\frac{u_\theta}{r}$ from equations (2.2.6) will yield the compatibility equation for ψ:

$$\frac{\partial^2\psi}{\partial r^2} - \frac{3}{r}\frac{\partial\psi}{\partial r} + \nu_3^2 \frac{\partial^2\psi}{\partial z^2} = 0 \ . \tag{2.2.7}$$

On the lateral surfaces the following boundary conditions must be satisfied:

$$\begin{aligned} \sigma_{r\theta}\, n_r + \sigma_{\theta z}\, n_z &= T_\theta^{(i)} \quad \text{on} \quad S_i \ , \\ \sigma_{r\theta}\, n_r + \sigma_{\theta z}\, n_z &= T_\theta^{(o)} \quad \text{on} \quad S_o \ , \end{aligned} \tag{2.2.8}$$

where n_α is the cosine of the angle between the α-axis and the outward unit normal $\underset{\sim}{n}$ at a point on the surface under consideration.

At an arbitrary section the transmitted torque is

$$M(z) = \iint ar\sigma_{\theta z}\, dA = 2\pi \int_{R_i(z)}^{R_o(z)} \frac{arc_{44}}{\nu_3}\frac{1}{r^2}\frac{\partial\psi}{\partial r}\, a^2 r dr$$

$$= \frac{2\pi c_{44} a^3}{\nu_3} \left[\psi(R_o(z),z) - \psi(R_i(z),z)\right] \ , \tag{2.2.9}$$

where

$R_i(z)$ = radius of the inner bounding surface at the section,

$R_o(z)$ = radius of the outer bounding surface at the section.

Where the transverse cross-section is a simply-connected two-dimensional region, $R_i(z) = 0$. At the ends, where the applied or reactant torque is known, equation (2.2.9) gives the (relaxed) end conditions.

The torsion problem thus becomes one of finding $\psi(r,z)$ satisfying equation (2.2.7) in a planar region R consisting of one half of a meridional section of B. (See Fig. 2.2.2.) It will thus be convenient to transform the traction boundary conditions on the lateral surfaces (2.2.8) to conditions on ψ on the surface generators, C_i and C_o. To this end it is convenient to define a dimensionless parameter s on the generators which measures arc length along C_i and C_o, scaled by the length factor a. For definiteness s is assumed to decrease with increasing z on C_i, and to increase with increasing z on C_o. (See Fig. 2.2.2.) Then one may write

$$n_r = \frac{dz}{ds} \quad , \quad n_z = -\frac{dr}{ds} \quad \text{on } C_i \text{ and } C_o \, . \tag{2.2.10}$$

Using equations (2.2.4) and (2.2.10), conditions (2.2.8) now become

$$\frac{d\psi}{ds} = -\frac{\nu_3}{c_{44}} \, r^2 \, T_\theta^{(i)} \quad \text{on} \quad C_i \quad ,$$

$$\frac{d\psi}{ds} = -\frac{\nu_3}{c_{44}} \, r^2 \, T_\theta^{(o)} \quad \text{on} \quad C_o \quad ,$$

or

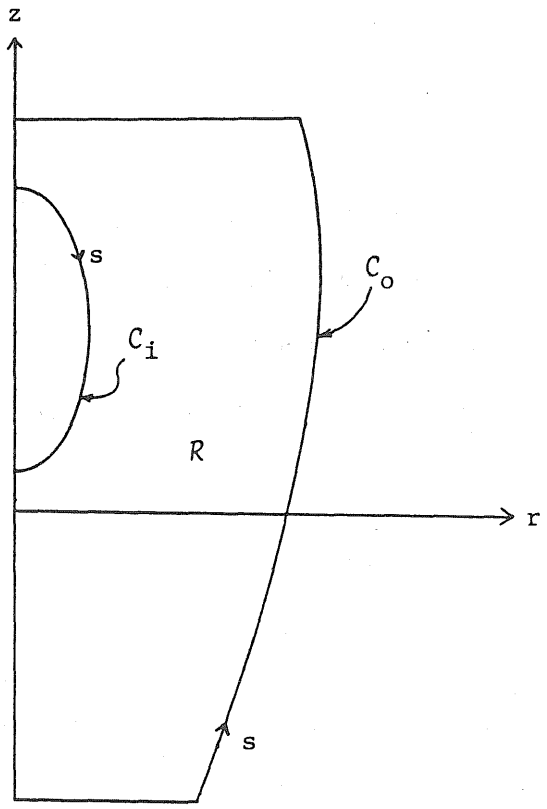

Fig. 2.2.2 Section in Meridional Half-Plane

$$\psi = -\frac{\nu_3}{c_{44}} \int_0^s T_\theta^{(i)} \, r^2 ds + c_i \quad \text{on} \quad C_i \ ,$$

$$\psi = -\frac{\nu_3}{c_{44}} \int_0^s T_\theta^{(o)} \, r^2 ds + c_o \quad \text{on} \quad C_o \ , \tag{2.2.11}$$

where c_i and c_o are constants. Thus, if the lateral surfaces are traction-free the stress function must be constant over each surface generator. When this is the case, equations (2.2.9) and (2.2.11) imply that the transmitted torque is constant throughout the body and is given by

$$M = \frac{2\pi c_{44} a^3}{\nu_3} (c_o - c_i) \ . \tag{2.2.12}$$

Since the stress field is uniquely defined by the stress function derivatives (equation (2.2.4)), a constant stress function may be added to the solution without affecting the stress state. This implies that ψ may always be adjusted in such a way that either c_i or c_o in equation (2.2.11) vanishes, thus allowing one of these constants to be taken as zero at the outset.

The problem of the torsion of a transversely isotropic body of revolution $\mathcal{B}$ can be reduced to that of an isotropic body occupying the transformed region $\mathcal{B}'$ by the change of variable

$$z_3 = \frac{z}{\nu_3} \ . \tag{2.2.13}$$

By formally making the substitutions $\psi(r,z) = \bar{\psi}(r,z_3)$ and $\frac{d}{ds} = \frac{ds_3}{ds}\frac{d}{ds_3}$ in equations (2.2.7) and (2.2.11), the boundary value problem for the new stress function $\bar{\psi}(r,z_3)$ in the transformed space becomes the following:

$$\frac{\partial^2\bar{\psi}}{\partial r^2} - \frac{3}{r}\frac{\partial\bar{\psi}}{\partial r} + \frac{\partial^2\bar{\psi}}{\partial z_3^2} = 0 \quad \text{in } R' \quad ; \tag{2.2.14}$$

$$\begin{aligned} \bar{\psi} &= -\frac{\nu_3}{c_{44}} \int_0^{s_3} \bar{T}_\theta^{(i)}\, r^2 ds_3 + \bar{c}_i \quad \text{on } C_i' \quad , \\ \bar{\psi} &= -\frac{\nu_3}{c_{44}} \int_0^{s_3} \bar{T}_\theta^{(o)}\, r^2 ds_3 + \bar{c}_o \quad \text{on } C_o' \quad , \end{aligned} \tag{2.2.15}$$

where R', C_i', C_o', and ds_3 are the images of R, C_i, C_o, and ds in the r-z_3 half-plane, $\bar{c}_i$ and $\bar{c}_o$ are constants, and

$$\begin{aligned} \bar{T}_\theta^{(i)} &= \frac{ds}{ds_3}\, T_\theta^{(i)} \quad , \\ \bar{T}_\theta^{(o)} &= \frac{ds}{ds_3}\, T_\theta^{(o)} \quad , \end{aligned} \tag{2.2.16}$$

are the components of fictitious traction vectors acting on C_i' and C_o', respectively. Note that the prescribed tractions on the actual body differ in magnitude from the fictitious tractions applied to the transformed body, but the forces acting on corresponding surface elements are identical,

i.e., $T_\theta \, ds(rd\theta) = \bar{T}_\theta \, ds_3(rd\theta)$. Equations (2.2.14) and (2.2.15) are the governing equations of the Michell-Föppl theory for the torsion of an isotropic body of revolution, with shear modulus $\frac{c_{44}}{\nu_3}$, occupying the region $\mathcal{B}'$, and subjected to tangential tractions $\bar{\underset{\sim}{T}}^{(i)} = \bar{T}_\theta^{(i)} \underset{\sim}{e}_\theta$ and $\bar{\underset{\sim}{T}}^{(o)} = \bar{T}_\theta^{(o)} \underset{\sim}{e}_\theta$ on its lateral surfaces. Thus for $0 < \nu_3 < \infty$, the transversely isotropic torsion problem corresponds to an isotropic torsion problem of different geometry and boundary conditions.

2.3 Extension of Stress Function Approach to Exterior Domains

For the case in which the region occupied by the transversely isotropic body is an infinite region exterior to a finite number of closed regular surfaces, the second of conditions (2.2.8) and (2.2.11) must be replaced by asymptotic conditions at infinity. The following conditions will ensure uniqueness:

$$\left.\begin{aligned} \sigma_{r\theta} &= \sigma_{r\theta}^{(0)} + O\left(\frac{1}{R^2}\right) , \\ \sigma_{\theta z} &= \sigma_{\theta z}^{(0)} + O\left(\frac{1}{R^2}\right) , \end{aligned}\right\} \quad \text{as } R \to \infty , \tag{2.3.1}$$

or

$$\psi = \psi_0 + O(R) \quad \text{as} \quad R \to \infty , \tag{2.3.2}$$

where R is the distance from the origin, $\sigma_{r\theta}^{(0)}$ and $\sigma_{\theta z}^{(0)}$ are the components of the prescribed stress field defined in the neighborhood of infinity, and ψ_0 the corresponding stress function. The $O(\frac{1}{R^2})$ behavior of the stress field at infinity, along with $O(\frac{1}{R})$ behavior of the displacements ($u_\theta = u_\theta^{(0)} + O(\frac{1}{R})$), enables one to extend Kirchhoff's classical uniqueness proof [26] to exterior domains, since these are sufficient conditions for the pertinent improper surface integrals to vanish.

In 1961 Gurtin and Sternberg [16] showed that for an <u>isotropic</u> body uniqueness is preserved if the regularity conditions (2.3.1) are relaxed to

$$\left.\begin{aligned} \sigma_{r\theta} &= \sigma_{r\theta}^{(0)} + o(1) \quad , \\ \sigma_{\theta z} &= \sigma_{\theta z}^{(0)} + o(1) \quad , \end{aligned}\right\} \quad \text{as } R \to \infty \tag{2.3.3}$$

thus eliminating the need to specify the <u>rate</u> of the asymptotic behavior in the problem formulation. Conditions (2.3.3) require only that the stresses tend uniformly to their prescribed values at infinity, and the authors mentioned have shown that, for isotropy, these relaxed conditions imply the $O(\frac{1}{R^2})$ behavior of the stresses at infinity. In view of the fact that the stress function formulation of the torsion problem for a transversely isotropic body of revolution is mathematically equivalent to that for an isotropic torsion problem of different geometry and boundary conditions (Section 2.2), and because this correspondence is one-to-one, it would

seem reasonable that conditions (2.3.1) for the transversely isotropic torsion problem could be relaxed to conditions (2.3.3), implying a corresponding relaxation of condition (2.3.2). However, for the present investigation conditions (2.3.1) and (2.3.2) will suffice.

CHAPTER 3

MATHEMATICAL FORMULATION OF THE STRESS INTERFERENCE PROBLEM

3.1 General

The purpose of the present chapter is to formulate the boundary value problem for the particular problem of the torsion of a transversely isotropic solid containing two spheroidal cavities. A pair of spheroidal coordinate systems are introduced to facilitate the mathematical description of the two cavities. Expressions are given which relate the coordinate parameters of one system to those of the other. The two systems are orthogonal in the (r, θ, z_3)-space, but not in the "physical" space. This is a desirable characteristic since the field equation governing the stress function is in canonical form in the transformed space, i.e., the (r, θ, z_3)-space. Choosing the systems in this way will enable one to obtain a pair of solution aggregates by the method of separation of variables.

3.2 Geometry and Coordinate Systems

The region of interest $\mathcal{B}$ is the unbounded region in the (r, θ, z)-space exterior to the two spheroidal surfaces

$$r^2 + \frac{(z \pm \lambda)^2}{\kappa^2} = 1 , \qquad \lambda \geq \kappa \tag{3.2.1}$$

where r and z are rendered dimensionless by a scale factor a. Thus, equation (3.2.1) represents two spheroids with semi-axes of lengths a and κa in the r-and z-directions, respectively, whose centers are separated by a distance $2\lambda a$ along the z-axis. (See Fig. 3.2.1.) The condition $\lambda \geq \kappa$ implies that the cavity surfaces intersect at, at most, one point.

It is convenient to introduce two spheroidal coordinate systems whose origins are located at the centers of the two cavities. These systems are defined through the following transformations:

$$\left.\begin{aligned} r &= \alpha(1 - p_1^2)^{\frac{1}{2}} (q_1^2 - 1)^{\frac{1}{2}} \quad , \\ z_3 - \lambda_3 &= \alpha p_1 q_1 \quad , \\ \theta &= \theta \quad ; \end{aligned}\right\} \tag{3.2.2}$$

$$\left.\begin{aligned} r &= \alpha(1 - p_2^2)^{\frac{1}{2}} (q_2^2 - 1)^{\frac{1}{2}} \quad , \\ z_3 + \lambda_3 &= -\alpha p_2 q_2 \quad , \\ \theta &= \theta \quad ; \end{aligned}\right\} \tag{3.2.3}$$

where

$$z_3 = \frac{z}{\nu_3} \quad , \qquad \lambda_3 = \frac{\lambda}{\nu_3} \quad , \qquad \kappa_3 = \frac{\kappa}{\nu_3} \quad ; \tag{3.2.4}$$

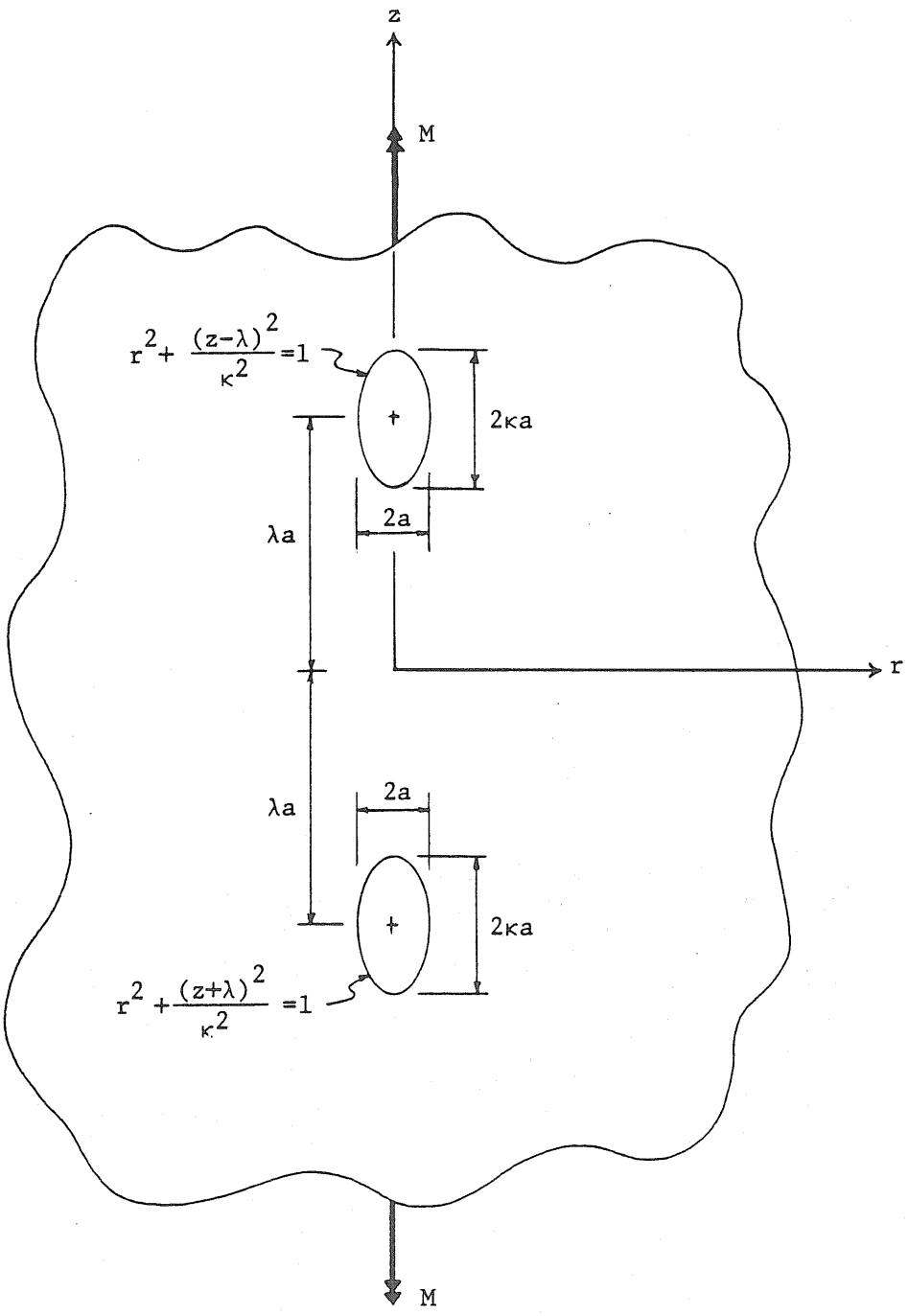

Fig. 3.2.1 Geometry of the Twin Cavity Problem

$$\alpha = \begin{cases} \sqrt{\kappa_3^2 - 1} & , \quad \kappa_3 > 1 \ , \\ -i\sqrt{1 - \kappa_3^2} & , \quad \kappa_3 < 1 \ , \end{cases} \tag{3.2.5}$$

$$p_j = \cos \gamma_j \quad , \qquad 0 \leq \gamma_j \leq \pi \ , \tag{3.2.6}$$

$$q_j = \begin{cases} \cosh \eta_j & , \quad \kappa_3 > 1 \quad , \\ i \sinh \eta_j & , \quad \kappa_3 < 1 \quad , \end{cases} \qquad 0 \leq \eta_j < \infty \quad , \quad j = 1, 2 \ . \tag{3.2.7}$$

The parameter α has been chosen in such a way that the cavity surfaces coincide with two coordinate surfaces, given by

$$q_1 = q_0 \quad , \qquad q_2 = q_0 \quad , \tag{3.2.8}$$

where

$$q_0 = \frac{\kappa_3}{\alpha} = \begin{cases} \dfrac{\kappa_3}{\sqrt{\kappa_3^2 - 1}} & , \quad \kappa_3 > 1 \ , \\ i \dfrac{\kappa_3}{\sqrt{1 - \kappa_3^2}} & , \quad \kappa_3 < 1 \ . \end{cases} \tag{3.2.9}$$

The region of interest $\mathcal{B}$ can now be described as the set of points for which both $|q_1| \geq |q_0|$ and $|q_2| \geq |q_0|$.

The transformation from the (p_1, q_1, θ)-system to the (p_2, q_2, θ)-system and its inverse are obtained by eliminating r and z_3 from equations (3.2.2) and (3.2.3):

$$\left.\begin{aligned} q_2 &= \hat{q}_2(p_1,q_1) = + \left[\frac{1}{2} \left(B_1 \pm \sqrt{B_1^2 - 4\,C_1^2}\right)\right]^{\frac{1}{2}} , \\ p_2 &= \hat{p}_2(p_1,q_1) = - \frac{C_1}{\hat{q}_2(p_1,q_1)} , \end{aligned}\right\} \tag{3.2.10}$$

where

$$\left.\begin{aligned} B_1 &= p_1^2 + q_1^2 + 2\beta\, p_1 q_1 + \beta^2 , \\ C_1 &= p_1 q_1 + \beta , \\ \beta &= \frac{2\lambda_3}{\alpha} . \end{aligned}\right\} \tag{3.2.11}$$

The inverse is obtained by interchanging subscripts "1" and "2". Where dual signs occur in equation (3.2.10), the upper sign is chosen when $\kappa_3 > 1$, the lower sign when $\kappa_3 < 1$. These choices give the systems a desired symmetry; namely that on $z = 0$,

$$q_2 = q_1 \quad , \quad p_2 = p_1 .$$

On $q_1 = q_0$ (the upper cavity surface), q_2, p_2, and p_1 take on the following values:

$$\left.\begin{aligned} q_2 = q_{20} \equiv \hat{q}_2(p_1,q_0) &= +\left[\frac{1}{2}\left(B_{10} \pm \sqrt{B_{10}^2 - 4C_{10}^2}\right)\right]^{\frac{1}{2}} , \\ p_2 = p_{20} \equiv \hat{p}_2(p_1,q_0) &= -\frac{C_{10}}{\hat{q}_2(p_1,q_0)} , \end{aligned}\right\} \tag{3.2.12}$$

$$p_1 = p_{10} \equiv \frac{z - \lambda}{\kappa} , \tag{3.2.13}$$

where

$$\left.\begin{aligned} B_{10} &= p_1^2 + q_0^2 + 2\beta p_1 q_0 + \beta^2 , \\ C_{10} &= p_1 q_0 + \beta . \end{aligned}\right\} \tag{3.2.14}$$

It is important to realize that the two spheroidal systems employed are each orthogonal in the (r, θ, z_3)-space, but not in the "physical" (r, θ, z)-space. In the transformed space these systems are two standard spheroidal systems -- two prolate spheroidal systems ($\kappa_3 > 1$) or two oblate spheroidal systems ($\kappa_3 < 1$) [33]. The traces of the coordinate surfaces in the meridional plane are plotted in Figure 3.2.2 for the case $\kappa_3 > 1$.

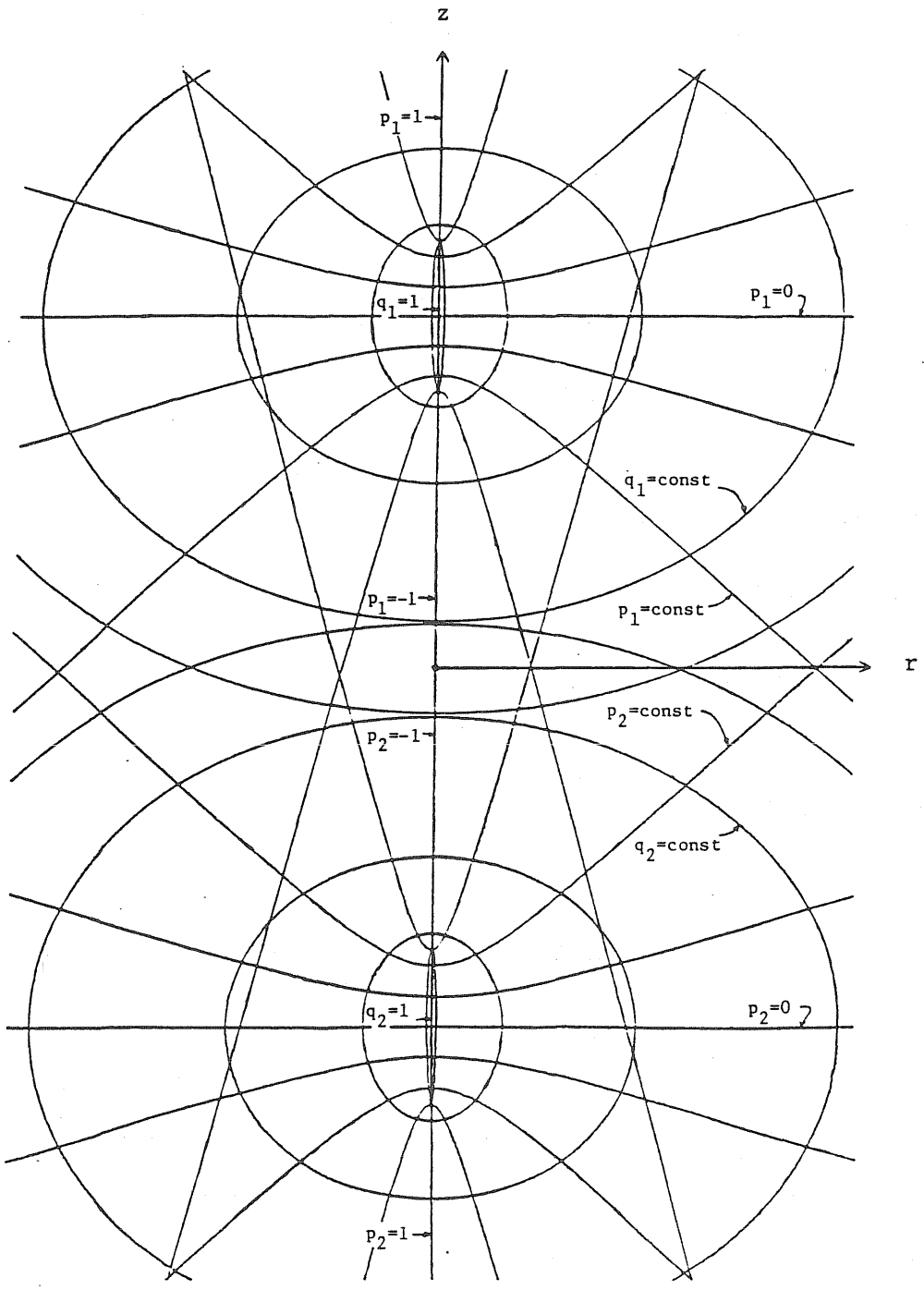

Fig. 3.2.2 Coordinate Surfaces in the Meridional Plane ($\kappa_3 > 1$)

3.3 Statement of the Boundary Value Problem

The boundary value problem for the torsion of a transversely isotropic solid containing two spheroidal cavities will now be formulated. The stress function ψ must satisfy the compatibility equation,

$$\frac{\partial^2\psi}{\partial r^2} - \frac{3}{r}\frac{\partial\psi}{\partial r} + \frac{\partial^2\psi}{\partial z_3^2} = 0 \qquad \text{in} \quad \mathcal{B} \ , \tag{3.3.1}$$

the boundary conditions,

$$\psi\big|_{q_1=q_0} = \psi\big|_{q_2=q_0} = 0 \ , \tag{3.3.2}$$

and the condition at infinity,

$$\psi = \psi_0 + O(R) = \frac{\nu_3 \tau a}{4} r^4 + O(R) \quad \text{as} \quad R \to \infty \ . \tag{3.3.3}$$

This last condition implies that the elastic state corresponding to ψ approaches the Saint-Venant solution for the torsion of a circular cylinder, at large distances from the perturbations. Here τ denotes the angle of twist per unit length.

Equations (3.3.1), (3.3.2), and (3.3.3) comprise the mathematical formulation of the problem at hand.

CHAPTER 4

SOLUTION OF THE STRESS INTERFERENCE PROBLEM

4.1 General

Chapter 4 begins by outlining the method of solution for the boundary value problem stated in the previous chapter. Since the problem is shown to reduce to the solution of an infinite system of linear algebraic equations, a trunction of this system is performed to yield an approximate solution. The equivalence of this truncated solution to that obtained through a method of weighted residuals or a virtual work formulation is shown. Explicit expressions are given for the corresponding stresses, stress concentration factors, and stress interference factors.

4.2 Method of Solution

Let

$$\psi = r^2 \Psi \tag{4.2.1}$$

Equations (3.2.2), (3.2.3), (3.3.1), and (4.2.1) yield the compatibility equation for Ψ in the (p_i, q_i, θ)-system $(i = 1,2)$:

$$(q_i^2 - 1)\frac{\partial^2 \Psi}{\partial q_i^2} + 2q_i \frac{\partial \Psi}{\partial q_i} - \frac{4\Psi}{q_i^2 - 1} + (1-p_i^2)\frac{\partial^2 \Psi}{\partial p_i^2} - 2p_i \frac{\partial \Psi}{\partial p_i} - \frac{4\Psi}{1-p_i^2} = 0 . \tag{4.2.2}$$

Separating variables in equation (4.2.2) one obtains the following solutions:

$$\psi_n = \begin{Bmatrix} P_n^2(p_i) & P_n^2(q_i) \\ & x \\ Q_n^2(p_i) & Q_n^2(q_i) \end{Bmatrix} , \qquad (4.2.3)$$

where $P_n^2(p_i)$ and $Q_n^2(q_i)$ are the associated Legendre functions of degree n and order 2, of the first and second kinds, respectively. Since $P_n^2(q_i)$ and $Q_n^2(p_i)$ are singular at points in the body (at $p_i = \pm 1$ and q_i = the point at infinity), these solutions must be eliminated. Thus, the aggregate of regular solutions becomes

$$\psi_n = r^2 \begin{Bmatrix} P_n^2(p_1) & Q_n^2(q_1) \\ & \\ P_n^2(p_2) & Q_n^2(q_2) \end{Bmatrix} , \quad n = 2, 3, 4, \ldots . \qquad (4.2.4)$$

Note that ψ_1 vanishes due to the fact that $P_1^2(p_i) = 0$.

Equation (3.3.1) is therefore satisfied by a solution of the form

$$\psi = \psi_0 - \frac{\nu_3 \tau a}{12} r^2 \sum_{n=2}^{\infty} A_n [P_n^2(p_1)Q_n^2(q_1) + P_n^2(p_2)Q_n^2(q_2)], \qquad (4.2.5)$$

where $\psi_0 = \frac{\nu_3 \tau a}{4} r^4$ corresponds to the uniform field given by the Saint-Venant solution for the torsion of a circular cylinder. Therefore,

the series portion of solution (4.2.5) represents the superposition of singularities (within the cavities) which are needed to remove the residual tractions on the cavity surfaces introduced by the uniform field. If it is assumed that this series converges uniformly and absolutely for $-1 \leq p_i \leq 1$ and $|q_0| \leq |q_i| < \infty$, then solution (4.2.5) satisfies the condition at infinity (3.3.3), since

$$\lim_{q_i \to \infty} P_n^2(p_i)\, Q_n^2(q_i) = 0 \quad .$$

The problem now becomes one of choosing the superposition parameters A_n to satisfy the boundary conditions (3.3.2).

Due to the symmetry inherent in the assumed form of solution, satisfying boundary conditions on one cavity guarantees that they are also satisfied on the other cavity. Thus, the boundary conditions reduce to

$$\psi\Big|_{q_1=q_0} = 0 \quad . \tag{4.2.6}$$

Using equation (4.2.5) and the expressions $r^2 = \frac{\alpha^2}{3}(q_1^2 - 1)P_2^2(p_1)$, $\alpha^2(q_0^2 - 1) = 1$, equation (4.2.6) becomes

$$P_2^2(p_1) - \sum_{n=2}^{\infty} A_n \{Q_n^2(q_0)P_n^2(p_1) + Q_n^2[\hat{q}_2(p_1,q_0)]P_n^2[\hat{p}_2(p_1,q_0)]\} = 0 \quad . \tag{4.2.7}$$

Expanding $Q_n^2\,[\hat{q}_2(p_1,q_0)]\;P_n^2[\hat{p}_2(p_1,q_0)]$ in a series of associated Legendre functions of order 2, equation (4.2.7) becomes

$$P_2^2(p_1) - \sum_{n=2}^{\infty} A_n[Q_n^2(q_0)P_n^2(p_1) + \sum_{m=2}^{\infty} a_n^{(m)}P_m^2(p_1)] = 0 \ ,$$

or

$$\sum_{n=2}^{\infty} [\delta_{2,n} - Q_n^2(q_0)\ A_n - \sum_{m=2}^{\infty} a_m^{(n)}A_m]\ P_n^2(p_1) = 0 \quad , \tag{4.2.8}$$

where

$$a_m^{(n)} = \frac{2n+1}{2}\,\frac{(n-2)!}{(n+2)!}\int_{-1}^{1} Q_m^2[\hat{q}_2(p_1,q_0)]P_m^2[\hat{p}_2(p_1,q_0)]\ P_n^2(p_1)\ dp_1 \quad , \tag{4.2.9}$$

$\hat{q}_2(p_1,q_0)$ and $\hat{p}_2(p_1,q_0)$ are given by equations (3.2.12), and $\delta_{2,n}$ is the Kronecker delta. The methods for computing the associated Legendre functions are described in the Appendix. Note that $a_m^{(n)}$ depends on κ_3 and λ_3.

Setting each coefficient of $P_n^2(p_1)$ equal to zero in equation (4.2.8), one arrives at the following system of linear algebraic equations to determine the coefficients of superposition A_n:

$$[Q_n^2(q_0) + a_n^{(n)}]\ A_n + \sum_{\substack{m=2 \\ m\neq n}}^{\infty} a_m^{(n)}A_m = \delta_{2,n}\ ,\ n = 2,\ 3,\ 4,\ \ldots\ . \tag{4.2.10}$$

Once the A_n are known, the stress field is found using equations (2.2.4). (See Section 4.6 for the explicit expressions.)

4.3 Alternate Representation for the Case $\kappa_3 < 1$

When $\kappa_3 < 1$ the spheroidal coordinate systems are oblate in the (r,θ,z_3)-space and α and q_j, $j = 1,2$, take on pure imaginary values. This gives pure imaginary values of $Q_n^2(q_j)$ and $a_n^{(m)}(\kappa_3,\lambda_3)$ for even n. In order to generate a real stress field, the stress function is required to be real. For this to be true, it is clear from equations (4.2.5) that A_n must be imaginary for even n and real for odd n. For computational purposes it will be convenient to reformulate equations (4.2.5), (4.2.9), and (4.2.10) in terms of real quantities only. To this end, the following are defined when $\kappa_3 < 1$:

$$\left.\begin{aligned}
&\alpha = -i\bar{\alpha}\ , \qquad \bar{\alpha} = \sqrt{1-\kappa_3^2}\ ,\\
&\beta = i\bar{\beta}\ , \qquad \bar{\beta} = \frac{2\lambda_3}{\bar{\alpha}}\ ,\\
&q_0 = i\bar{q}_0\ , \qquad \bar{q}_0 = \frac{\kappa_3}{\sqrt{1-\kappa_3^2}}\ ,\\
&q_j = i\bar{q}_j\ , \qquad Q_n^2(q_j) = i^{n+1}\,\bar{Q}_n^2(\bar{q}_j)\ ,\\
&a_m^{(n)} = i^{m+1}\bar{a}_m^{(n)}\ , \quad A_n = i^{n+1}\,\bar{A}_n\ .
\end{aligned}\right\} \qquad (4.3.1)$$

Thus, all "barred terms" represent real constants, real variables, or real-valued functions of a real variable. The necessary equations can now be written in modified form:

$$\psi = \psi_0 + \frac{\nu_3 \tau a}{12} r^2 \sum_{n=2}^{\infty} (-1)^n \bar{A}_n [P_n^2(p_1)\bar{Q}_n^2(\bar{q}_1) + P_n^2(p_2)\bar{Q}_n^2(\bar{q}_2)] \; ; \qquad (4.3.2)$$

$$(-1)^n [\bar{Q}_n^2(\bar{q}_0) + \bar{a}_n^{(n)}]\bar{A}_n + \sum_{\substack{m=2 \\ m\neq n}}^{\infty} (-1)^m \bar{a}_m^{(n)} \bar{A}_m = -\delta_{2,n} \quad n=2,3,4,\ldots \qquad (4.3.3)$$

The Legendre coefficients $\bar{a}_m^{(n)}$ are given by

$$\bar{a}_m^{(n)} = \frac{1}{i^{m+1}} a_m^{(n)} = \frac{2n+1}{2} \frac{(n-2)!}{(n+2)!} \int_{-1}^{1} \bar{Q}_m^2[\hat{\bar{q}}_2(p_1,\bar{q}_0)] \, P_m^2[\hat{\bar{p}}_2(p_1,\bar{q}_0)] P_n^2(p_1) dp_1 \; , \qquad (4.3.4)$$

where

$$\left.\begin{aligned} \hat{\bar{q}}_2(p_1,\bar{q}_0) &= [\frac{1}{2}(\sqrt{\bar{B}_{10}^2 + 4\bar{C}_{10}^2} - \bar{B}_{10})]^{\frac{1}{2}} \; , \\ \hat{\bar{p}}_2(p_1,\bar{q}_0) &= -\frac{\bar{C}_{10}}{\hat{\bar{q}}_2(p_1,\bar{q}_0)} \; , \end{aligned}\right\} \qquad (4.3.5)$$

$$\left.\begin{aligned} \bar{B}_{10} &= p_1^2 - 2\bar{\beta}\,\bar{q}_0\,p_1 - (\bar{q}_0^2 + \bar{\beta}^2) \quad , \\ \bar{C}_{10} &= \bar{q}_0 p_1 + \bar{\beta} \quad . \end{aligned}\right\} \tag{4.3.6}$$

The computation of $\bar{Q}_m^2(\bar{q})$, $\bar{q} > 0$, is described in the Appendix.

4.4 Truncated Solution - Method of Weighted Residuals

Let $A_n^{(N)}$ and $\bar{A}_n^{(N)}$, $n = 2,3,\ldots,N$, denote the solution vectors of systems (4.2.10) and (4.3.3) truncated after $n = N$, and $\psi^{(N)}$ the corresponding stress function:

$$\psi^{(N)} = \begin{cases} \psi_0 - \dfrac{\nu_3 \tau a}{12}\, r^2 \sum\limits_{n=2}^{N} A_n^{(N)} [P_n^2(p_1)Q_n^2(q_1) + P_n^2(p_2)Q_n^2(q_2)], & \kappa_3 > 1; \quad (4.4.1) \\ \psi_0 + \dfrac{\nu_3 \tau a}{12}\, r^2 \sum\limits_{n=2}^{N} (-1)^n \bar{A}_n^{(N)} [P_n^2(p_1)\bar{Q}_n^2(\bar{q}_1) + P_n^2(p_2)\bar{Q}_n^2(\bar{q}_2)], & \kappa_3 < 1; \quad (4.4.2) \end{cases}$$

where $A_n^{(N)}$ and $\bar{A}_n^{(N)}$ satisfy the truncated systems

$$[Q_n^2(q_0) + a_n^{(n)}]A_n^{(N)} + \sum_{\substack{m=2 \\ m\neq n}}^{N} a_m^{(n)} A_m^{(N)} = \delta_{2,n} \quad , \qquad n = 2,3,\ldots,N; \tag{4.4.3}$$

$$(-1)^n[\bar{Q}_n^2(\bar{q}_0) + \bar{a}_n^{(n)}]\bar{A}_n^{(N)} + \sum_{\substack{m=2 \\ m\neq n}}^{N} (-1)^m \bar{a}_m^{(n)}\bar{A}_m^{(N)} = -\delta_{2,n} \quad , \quad n = 2,3,\ldots,N \; . \tag{4.4.4}$$

It will now be shown that the above solution is equivalent to the approximate solution obtained by a method of weighted residuals.

For the case $\kappa_3 > 1$ take the stress function in the form of equation (4.4.1), where the $A_n^{(N)}$ are a finite number of unknown parameters whose values will be chosen to given the "best" approximation in some sense. For an exact solution, the stress function must satisfy boundary condition (4.2.6), which in this case becomes

$$\psi^{(N)}\Big|_{q_1=q_0} = \frac{\nu_3 \tau a}{12}(1-p_1^2)\{P_2^2(p_1) - \sum_{n=2}^{N} A_n^{(N)}[Q_n^2(q_0)P_n^2(p_1) + Q_n^2(q_{20})P_n^2(p_{20})]\} \tag{4.4.5}$$

$$|p_1| \leq 1 \; .$$

Since the series in the above equation would most likely have to be infinite in order to satisfy the boundary condition at all points on the cavity surfaces, condition (4.4.5) must be satisfied in an approximate fashion. One method of doing this is to choose the $A_n^{(N)}$ in such a way that the integrals of the residual stress function $\psi^{(N)}\Big|_{q_1=q_0}$ multiplied by a family of weighting functions over the boundary will vanish:

$$\int_{-1}^{1} \psi^{(N)}\Big|_{q_1=q_0} W_m(p_1)\, dp_1 = 0 \quad , \quad m = 2,3,\ldots,N \; . \tag{4.4.6}$$

If the weighting functions are taken as

$$W_m(p_1) = P_m''(p_1) = \frac{P_m^2(p_1)}{1-p_1^2} \quad , \tag{4.4.7}$$

where $P_m(p_1)$ is the m^{th}-degree Legendre polynomial and primes denote differentation, then the relaxed boundary condition (4.4.6) becomes

$$\int_{-1}^{1} P_2^2(p_1)P_m^2(p_1)dp_1 - \sum_{n=2}^{N} A_n^{(N)} [Q_n^2(q_0)\int_{-1}^{1} P_n^2(p_1)P_m^2(p_1)dp_1 + \int_{-1}^{1} Q_n^2(q_{20})P_n^2(p_{20})P_m^2(p_1)dp_1] = 0 \quad , \tag{4.4.8}$$

$$m = 2,3,\ldots,N \ .$$

Using the orthogonality condition

$$\int_{-1}^{1} P_m^2(p_1)P_n^2(p_1)dp_1 = \frac{2}{2n+1}\frac{(n+2)!}{(n-2)!}\ \delta_{n,m}$$

and definition (4.2.9), condition (4.4.8) reduces to

$$[Q_n^2(q_0) + a_n^{(n)}]\ A_n^{(N)} + \sum_{\substack{m=2 \\ m\neq n}}^{N} a_m^{(n)}\ A_m^{(N)} = \delta_{2,n} \quad , \quad n = 2,3,\ldots,N \ ,$$

which is identical to the truncated system given by equation (4.4.3). In a similar way the solution given by equations (4.4.2) and (4.4.4) can be shown to be a weighted residuals solution.

In the next section it is shown that the conditions on the weighted stress function residuals can be related to the more intuitive concept of residual surface traction and the principle of virtual work.

4.5 Virtual Work Interpretation of Truncated Solution

The condition on the residual stress function (equations (4.4.6) and (4.4.7)), which is implied by the truncation of system (4.2.10) or (4.3.3), may be integrated by parts:

$$\int_{-1}^{1} \psi^{(N)}\Big|_{q_1=q_0} P_m''(p_1)dp_1 = [\psi^{(N)}\Big|_{q_1=q_0} P_m'(p_1)]_{-1}^{1} - \int_{-1}^{1} \frac{d}{dp_1}[\psi^{(N)}\Big|_{q_1=q_0}]P_m'(p_1)dp_1 = 0, \qquad m = 2,3,\ldots,N . \tag{4.5.1}$$

Since the stress function vanishes at the poles, this becomes

$$\int_{-1}^{1} \frac{d}{dp_1}[\psi^{(N)}\Big|_{q_1=q_0}] P_m'(p_1)dp_1 = 0 \quad , \quad m = 2,3,\ldots,N . \tag{4.5.2}$$

The non-vanishing component of surface traction $T_\theta^{(N)}(p_1)$, the residual traction, can be shown to depend only on the values of the stress function derivative along the boundary:

$$T_\theta^{(N)}(p_1) = \sigma_{r\theta}^{(N)} \frac{dr}{dn} + \sigma_{\theta z}^{(N)} \frac{dz}{dn} = -\frac{c_{44}}{\nu_3 r^2}\left[\frac{\partial \psi^{(N)}}{\partial z}\frac{dz}{ds} + \frac{\partial \psi^{(N)}}{\partial r}\frac{dr}{ds}\right]$$

$$= -\frac{c_{44}}{\nu_3 r^2}\frac{d\psi^{(N)}}{ds} = -\frac{c_{44}}{\nu_3 r^2}\frac{dp_1}{ds}\frac{d\psi^{(N)}}{dp_1}\Bigg|_{q_1=q_0}$$

$$= -\frac{c_{44}}{\nu_3}\frac{1}{(1-p_1^2)^{1/2}[\kappa^2 + (1-\kappa^2)p_1^2]^{1/2}}\frac{d\psi^{(N)}}{dp_1}\Bigg|_{q_1=q_0} . \qquad (4.5.3)$$

Equations (4.5.2) and (4.5.3) imply

$$\int_{-1}^{1} T_\theta^{(N)}(p_1)\{[\kappa^2 + (1-\kappa^2)p_1^2]^{1/2} P_m^1(p_1)\}\, dp_1 = 0, \quad m = 2,3,\ldots,N . \qquad (4.5.4)$$

Let

$$\delta u_\theta^{(m)}(p_1) \equiv \delta\beta_m P_m^1(p_1) , \qquad (4.5.5)$$

where $\delta\beta_m$ is small, be the boundary values of a set of virtual displacement fields. Then, using the expression $dS = a^2[\kappa^2 + (1-\kappa^2)p_1^2]^{1/2}\, dp_1\, d\theta$ for the differential element of surface area on the upper cavity surface, equation (4.5.4) may be written as

$$\iint_{q_1=q_0} T_\theta^{(N)} \, \delta u_\theta^{(m)} \, dS = 0 \ , \quad m = 2,3, \ldots , N \ , \tag{4.5.6}$$

or the virtual work of the residual surface tractions through a finite number of virtual boundary displacements vanishes. (Equation (4.5.6) is identically satisfied for m = 1, which may be seen by inserting $P_1''(p_1) = 0$ in equation (4.5.1).) It will now be shown that equation (4.5.6) indeed expresses the principle of virtual work, where the set of admissible displacement fields is limited to those having the form of equation (4.5.5) on the upper cavity, which vanish at infinity, and which are antisymmetric about z = 0, in addition to satisfying the necessary smoothness requirements.

Consider the following traction boundary value problem: Let $\mathcal{B}_R$ denote a homogeneous elastic body bounded by M closed regular surfaces S_1, S_2,..., S_M, and a spherical surface Σ_R of radius R, which encloses all of the S_m. Σ_R is assumed to be traction-free, while self-equilibrated tractions $\hat{t}_i$ are prescribed on each of the S_m. Assume the body force field vanishes. Then the principle of virtual work for this problem may be stated as follows:

$$\sum_{m=1}^{M} \int_{S_m} \hat{t}_i \, \delta u_i \, dS = \int_{\mathcal{B}_R} \sigma_{ij} \, \delta \varepsilon_{ij} \, dV \ , \tag{4.5.7}$$

where δu_i is a small arbitrary virtual displacement field of sufficient smoothness and $\delta \varepsilon_{ij}$ the corresponding strain field. If the limit is taken as $R \to \infty$, equation (4.5.7) becomes

$$\sum_{m=1}^{M} \int_{S_m} \hat{t}_i \, \delta u_i \, dS = \lim_{R\to\infty} \int_{\mathcal{B}_R} \sigma_{ij} \, \delta\varepsilon_{ij} \, dV \quad , \tag{4.5.8}$$

where the limit is assumed to exist, and δu_i is assumed to vanish at infinity, thus eliminating rigid body displacements. For an exact solution σ_{ij} must satisfy equation (4.5.8) for all kinematically admissible δu_i. Now, if an approximate solution $\sigma_{ij}^{(N)}$ is assumed to be a linear combination of N known equilibrated stress fields, then $\sigma_{ij}^{(N)}$ can be expected to satisfy equation (4.5.8) for only N choices of δu_i:

$$\sum_{m=1}^{M} \int_{S_m} \hat{t}_i \, \delta u_i^{(n)} \, dS = \lim_{R\to\infty} \int_{\mathcal{B}_R} \sigma_{ij}^{(N)} \delta\varepsilon_{ij}^{(n)} \, dV \quad , \quad n = 1,2,\ldots,N \; . \tag{4.5.9}$$

Multiplying the homogeneous equilibrium equations for $\sigma_{ij}^{(N)}$ by $\delta u_i^{(n)}$, integrating over $\mathcal{B}_R$, and taking the appropriate limits yields the following:

$$\lim_{R\to\infty} \int_{\mathcal{B}_R} \sigma_{ij}^{(N)} \delta\varepsilon_{ij}^{(n)} dV = \sum_{m=1}^{M} \int_{S_m} \sigma_{ij}^{(N)} n_j \, \delta u_i^{(n)} dS + \lim_{R\to\infty} \int_{\Sigma_R} \sigma_{ij}^{(N)} n_j \delta u_i^{(n)} dS \; . \tag{4.5.10}$$

Equations (4.5.9) and (4.5.10) imply

$$\sum_{m=1}^{M} \int_{S_m} (\hat{t}_i - \sigma_{ij}^{(N)} n_j) \, \delta u_i^{(n)} dS = \lim_{R\to\infty} \int_{\Sigma_R} \sigma_{ij}^{(N)} n_j \, \delta u_i^{(n)} dS \quad . \tag{4.5.11}$$

If $\sigma_{ij}^{(N)} = O(\frac{1}{R^2})$ as $R \to \infty$, the R.H.S. vanishes to give

$$\sum_{m=1}^{M} \int_{S_m} (\hat{t}_i - t_i^{(N)})\, \delta u_i^{(n)} dS = 0 \ , \quad n = 1,2,\ldots,N \ , \tag{4.5.12}$$

where $t_i^{(N)} = \sigma_{ij}^{(N)} n_j$.

The auxiliary problem related to the stress interference problem for torsion is a particular case of the boundary value problem described above. (In the auxiliary problem the uniform torsion field is removed.) Therefore, the principle of virtual work (in the approximate sense) for the problem at hand reduces to equation (4.5.11), or

$$-2 \iint_{q_1=q_0} T_\theta^{(N)} \delta u_\theta^{(n)} \, dS = \lim_{R\to\infty} \int_{\Sigma_R} (\sigma_{r\theta}^{(N)} n_r + \sigma_{\theta z}^{(N)} n_z) \delta u_\theta^{(n)} dS \ .$$

It can be shown that the approximate stresses $\sigma_{r\theta}^{(N)}$ and $\sigma_{\theta z}^{(N)}$ for the auxiliary problem (derived from $\psi^{(N)} - \psi_0$) are of order $\frac{1}{R^4}$ at infinity, thus causing the limit on the R.H.S. to vanish. As a result, the principle of virtual work for the stress interference problem reduces to equation (4.5.6). Thus, the truncation process performed on the infinite set of equations may be viewed as a boundary residual method on the stress function or on the surface traction, or as a solution technique based on the principle of virtual work.

4.6 Expressions for the Elastic Field Quantities

In view of the symmetry of the posed problem, the stress field will be expressed in the (p_1,q_1,θ)-system only. By using the coordinate transformations given by equations (3.2.2) and (3.2.3), as well as equations (2.2.4) and (4.4.1), the stress field may be shown to be of the following form:

$$\left.\begin{aligned}
\sigma_{r\theta}^{(N)} = \frac{\nu_3 c_{66} \tau a}{12\alpha} \sum_{n=2}^{N} A_n^{(N)} \{ & \frac{1}{q_1^2 - p_1^2} [q_1(1-p_1^2) P_n^{2'}(p_1)\, Q_n^2(q_1) \\
& + p_1(q_1^2-1) P_n^2(p_1) Q_n^{2'}(q_1)] \\
& - \frac{1}{q_2^2 - p_2^2} [q_2(1-p_2^2) P_n^{2'}(p_2)\, Q_n^2(q_2) \\
& + p_2(q_2^2-1) P_n^2(p_2) Q_n^{2'}(q_2)]\} \\
\sigma_{\theta z}^{(N)} = \frac{c_{44} \tau a}{12} \{ & 12r - \frac{2}{r} \sum_{n=2}^{N} A_n^{(N)} [P_n^2(p_1) Q_n^2(q_1) + P_n^2(p_2) Q_n^2(q_2)] \\
& - \frac{r}{\alpha^2} \sum_{n=2}^{N} A_n^{(N)} \{ \frac{1}{q_1^2 - p_1^2} [-p_1 P_n^{2'}(p_1) Q_n^2(q_1) + q_1 P_n^2(p_1) Q_n^{2'}(q_1)] \\
& + \frac{1}{q_2^2 - p_2^2} [-p_2 P_n^{2'}(p_2)\, Q_n^2(q_2) + q_2 P_n^2(p_2) Q_n^{2'}(q_2)]\}\}
\end{aligned}\right\} \quad (4.6.1)$$

where $p_2 = \hat{p}_2(p_1,q_1)$ and $q_2 = \hat{q}_2(p_1,q_1)$ are given by equation (3.2.10), $r = \alpha(1 - p_1^2)^{\frac{1}{2}}(q_1^2 - 1)^{\frac{1}{2}}$, and $\sigma_{ij}^{(N)}$ is the stress field corresponding to $\psi^{(N)}$.

For computational purposes it will be convenient to write equations (4.6.1) in terms of $P_n^2(p_i)$ and $Q_n^2(q_i)$ only, rather than their derivatives. This can be accomplished by employing the following recurrence formulae [30]:

$$\frac{d\,P_n^2(x)}{dx} = \frac{1}{x^2-1}\,[nxP_n^2(x) - (n+2)P_{n-1}^2(x)] \quad , \qquad n = 2,3, \ldots ,$$

$$\frac{d\,Q_n^2(x)}{dx} = \frac{1}{x^2-1}\,[nxQ_n^2(x) - (n+2)Q_{n-1}^2(x)] \quad , \qquad n = 3,4, \ldots . \tag{4.6.2}$$

The second of these formulae is valid for n=2 if $Q_1^2(x)$ is defined by

$$Q_1^2(x) = \frac{2}{x^2-1} \quad . \tag{4.6.3}$$

(The usual definition is $Q_1^2(x) = \frac{3}{x^2-1}$.) Using equations (4.6.1)-(4.6.3) and evaluating the resulting expressions on $q_1=q_0$, one obtains the stress field at the upper cavity surface:

$$\left.\frac{\sigma_{r\theta}^{(N)}}{c_{44}\tau a}\right|_{q_1=q_0} = \frac{1}{12\nu_3\alpha}\sum_{n=2}^{N} A_n^{(N)}(n+2)\{\frac{1}{q_0^2-p_1^2}[q_0P_{n-1}^2(p_1)Q_n^2(q_0) - p_1P_n^2(p_1)Q_{n-1}^2(q_0)] - \frac{1}{q_2^2-p_2^2}[q_2P_{n-1}^2(p_2)Q_n^2(q_2) - p_2P_n^2(p_2)Q_{n-1}^2(q_2)]\} \tag{4.6.4.a}$$

$$\left.\frac{\sigma_{\theta z}^{(N)}}{c_{44}\tau a}\right|_{q_1=q_0} = (1-p_1^2)^{\frac{1}{2}}[[1-\sum_{n=2}^{N} A_n^{(N)}\{\frac{1}{2P_2^2(p_1)}[Q_n^2(q_0)P_n^2(p_1) + Q_n^2(q_2)P_n^2(p_2)] + \frac{1}{12\alpha^2}\{\frac{1}{q_0^2-p_1^2}[-\frac{p_1}{p_1^2-1}Q_n^2(q_0)(np_1P_n^2(p_1) - (n+2)P_{n-1}^2(p_1)) + \frac{q_0}{q_0^2-1}P_n^2(p_1)(nq_0Q_n^2(q_0) - (n+2)Q_{n-1}^2(q_0)) + \frac{1}{q_2^2-p_2^2}[-\frac{p_2}{p_2^2-1}Q_n^2(q_2)(np_2P_n^2(p_2) - (n+2)P_{n-1}^2(p_2)) + \frac{q_2}{q_2^2-1}P_n^2(p_2)(nq_2Q_n^2(q_2) - (n+2)Q_{n-1}^2(q_2))]\}\}] \tag{4.6.4.b}$$

where $p_2 = \hat{p}_2(p_1,q_0)$ and $q_2 = \hat{q}_2(p_1,q_0)$.

When $\kappa_3 < 1$, equations (4.6.4) involve imaginary terms on the right-hand side. To express the boundary stresses in terms of real quantities only, equations (4.3.1) are substituted into equations (4.6.4) to yield the following:

$$\left.\frac{\sigma_{r\theta}^{(N)}}{c_{44}\tau a}\right|_{q_1=q_0} = -\frac{1}{12\nu_3\bar{\alpha}}\sum_{n=2}^{N}(-1)^n\bar{A}_n^{(N)}(n+2)\{\frac{1}{\bar{q}_0^2+p_1^2}[\bar{q}_0P_{n-1}^2(p_1)\bar{Q}_n^2(\bar{q}_0) + p_1P_n^2(p_1)\bar{Q}_{n-1}^2(\bar{q}_0)] - \frac{1}{\bar{q}_2^2+p_2^2}[\bar{q}_2P_{n-1}^2(p_2)\bar{Q}_n^2(\bar{q}_2) + p_2P_n^2(p_2)\bar{Q}_{n-1}(\bar{q}_2)]\} \quad , \tag{4.6.5.a}$$

$$\left.\frac{\sigma_{\theta z}^{(N)}}{c_{44}\tau a}\right|_{q_1=q_0} = (1-p_1^2)^{\frac{1}{2}}[\![1+\sum_{n=2}^{N}(-1)^n\bar{A}_n^{(N)}\{\frac{1}{2P_2^2(p_1)}[\bar{Q}_n^2(\bar{q}_0)P_n^2(p_1) + \bar{Q}_n^2(\bar{q}_2)P_n^2(p_2)] + \frac{1}{12\bar{\alpha}^2}\{\frac{1}{\bar{q}_0^2+p_1^2}[\frac{p_1}{1-p_1^2}\bar{Q}_n^2(\bar{q}_0)(np_1P_n^2(p_1) - (n+2)P_{n-1}^2(p_1)) + \frac{\bar{q}_0}{\bar{q}_0^2+1}P_n^2(p_1)(n\bar{q}_0\bar{Q}_n^2(\bar{q}_0) + (n+2)\bar{Q}_{n-1}^2(\bar{q}_0))] + \frac{1}{\bar{q}_2^2+p_2^2}[\frac{p_2}{1-p_2^2}\bar{Q}_n^2(\bar{q}_2)(np_2P_n^2(p_2) - (n+2)P_{n-1}^2(p_2)) + \frac{\bar{q}_2}{\bar{q}_2^2+1}P_n^2(p_2)(n\bar{q}_2\bar{Q}_n^2(\bar{q}_2) + (n+2)\bar{Q}_{n-1}^2(\bar{q}_2))]\}\}]\!] \quad , \tag{4.6.5.b}$$

where $p_2 = \hat{\bar{p}}_2(p_1,\bar{q}_0)$ and $\bar{q}_2 = \hat{\bar{q}}_2(p_1,\bar{q}_0)$ are given by equations (4.3.5) and $\bar{A}_n^{(N)}$ satisfies system (4.4.4).

Since the maximum shear stress at the cavity surface will occur on planes normal to the boundary, and the coordinate surfaces $q_1 = q_0$ and

p_1 = constant are not orthogonal, it would be advantageous to obtain stress components with respect to an orthogonal spheroidal system. For this purpose a conventional spheroidal coordinate system, centered at $z = \lambda$, is introduced:

$$\left.\begin{aligned} r &= \alpha_0(1-p^2)^{\frac{1}{2}}\,(q^2-1)^{\frac{1}{2}} \quad , \\ z-\lambda &= \alpha_0 pq \quad . \end{aligned}\right\} \tag{4.6.6}$$

If

$$\alpha_0 \equiv \begin{cases} \sqrt{\kappa^2-1} & , \quad \kappa > 1 \ , \\ -i\sqrt{1-\kappa^2} & , \quad \kappa < 1 \ , \end{cases}$$

then the upper cavity surface $q_1 = q_0$ may also be represented by

$$q = \frac{\kappa}{\alpha_0} = \begin{cases} \dfrac{\kappa}{\sqrt{\kappa^2-1}} & , \quad \kappa > 1 \ , \\ i\,\dfrac{\kappa}{\sqrt{1-\kappa^2}} & , \quad \kappa < 1 \ . \end{cases}$$

The running variable on the cavity surface is identical to that in the non-orthogonal system:

$$p = p_1 = \frac{z - \lambda}{\kappa} \qquad \text{on} \quad q_1 = q_0 \ .$$

Transformation (4.6.6) implies the following stress transformation on the boundary:

$$\left.\begin{aligned} \sigma^{(N)}_{p\theta}\Big|_{q_1=q_0} &= \frac{1}{[\kappa^2 - (\kappa^2-1)p^2]^{\frac{1}{2}}} \Big[-p\sigma^{(N)}_{r\theta}\Big|_{q_1=q_0} \\ &\qquad + \kappa(1-p^2)^{\frac{1}{2}}\, \sigma^{(N)}_{\theta z}\Big|_{q_1=q_0}\Big] \ , \\ \sigma^{(N)}_{q\theta}\Big|_{q_1=q_0} &= \frac{1}{[\kappa^2 - (\kappa^2-1)p^2]^{\frac{1}{2}}} \Big[\kappa(1-p^2)^{\frac{1}{2}}\, \sigma^{(N)}_{r\theta}\Big|_{q_1=q_0} \\ &\qquad + p\sigma^{(N)}_{\theta z}\Big|_{q_1=q_0}\Big] \ . \end{aligned}\right\} \qquad (4.6.7)$$

For a spherical cavity, $\kappa = 1$, and these expressions reduce to the familiar stress transformation from circular cylindrical to spherical components, with $p = \cos\Theta$, where Θ is the azimuthal angle measured from the outer pole.

For an exact solution

$$\sigma_{q\theta}\Big|_{q_1=q_0} = -T_\theta = 0 \ ,$$

since the boundary is traction-free. Thus, the ultimate check on the accuracy of the truncated solution is that

$$\sigma_{q\theta}^{(N)} \Big|_{q_1=q_0} \sim 0 \quad .$$

As mentioned in Section 2.2, there exists a line integral representation for the angle of twist

$$\omega \equiv \frac{u_\theta}{r} \quad .$$

This representation will now be derived. Equations (2.2.6) may be written as

$$\frac{\partial \psi}{\partial r} = r^3 \frac{\partial \omega}{\partial z_3} \quad ,$$

$$\frac{\partial \psi}{\partial z_3} = -r^3 \frac{\partial \omega}{\partial r} \quad ,$$

enabling one to write the following:

$$r^3 d\omega = r^3 \left[\frac{\partial \omega}{\partial r} \, dr + \frac{\partial \omega}{\partial z_3} \, dz_3 \right] = - \frac{\partial \psi}{\partial z_3} \, dr + \frac{\partial \psi}{\partial r} \, dz_3 \quad .$$

Using transformations (3.2.2) and (3.2.3), this may be expressed in terms of p_i and q_i:

$$r^3 d\omega = \pm \left[\left(\frac{q_i^2 - 1}{1 - p_i^2} \right)^{1/2} \frac{\partial \psi}{\partial q_i} \, dp_i - \left(\frac{1 - p_i^2}{q_i^2 - 1} \right)^{1/2} \frac{\partial \psi}{\partial p_i} \, dq_i \right] \quad , \qquad (4.6.8)$$

where the upper sign is chosen for i = 1, the lower sign for i = 2. The left-hand side of this equation may also be expressed as

$$r^3 d\omega = r^3 \left(\frac{\partial \omega}{\partial p_i} \, dp_i + \frac{\partial \omega}{\partial q_i} \, dq_i \right) . \tag{4.6.9}$$

From equations (4.6.8) and (4.6.9) it can be concluded that

$$\left.\begin{aligned} \frac{\partial \omega}{\partial p_i} &= \pm \frac{1}{\alpha^3 (q_i^2 - 1)(1 - p_i^2)^2} \, \frac{\partial \psi}{\partial q_i} \quad , \\ \frac{\partial \omega}{\partial q_i} &= \mp \frac{1}{\alpha^3 (1 - p_i^2)(q_i^2 - 1)^2} \, \frac{\partial \psi}{\partial p_i} \quad . \end{aligned}\right\} \quad , \quad i = 1,2 \, . \tag{4.6.10}$$

If the stress function $\psi^{(N)}$ of equation (4.4.1) is broken up into three parts, ψ_0, ψ_1, and ψ_2, where ψ_0 is the uniform field and

$$\psi_i = - \frac{\nu_3 \tau a}{12} \, r^2 \sum_{n=2}^{N} A_n^{(N)} \, P_n^2(p_i) \, Q_n^2(q_i) \quad , \quad i = 1,2 \quad ,$$

and the contributions of each of these functions to the angle of twist are designated by ω_0, ω_1, and ω_2, then one may evaluate ω in the following manner:

$$\omega(P) = \omega_0 + \omega_1 + \omega_2 = \tau a z + \int_{\Gamma_1} d\omega_1 + \int_{\Gamma_2} d\omega_2 \quad ,$$

where Γ_1 and Γ_2 are paths within the body which begin at any point on the plane $z = 0$, i.e., where the angle of twist vanishes, and terminate at the point of interest P. Convenient choices of these paths would be arcs in the meridional plane along which a coordinate parameter remains constant, as shown in Figure 4.6.1. If the point P corresponds to coordinates $(\tilde{r},\tilde{z})$, $(\tilde{p}_1,\tilde{q}_1)$, or $(\tilde{p}_2,\tilde{q}_2)$, these paths of integration enable the angle of twist to be given by

$$\omega(P) = \tau a\tilde{z} + \int_{\lambda/\nu_3\alpha\tilde{q}_1}^{\tilde{p}_1} \frac{\partial\omega_1}{\partial p_1}\bigg|_{q_1=\tilde{q}_1} dp_1 + \int_{\lambda/\nu_3\alpha\tilde{q}_2}^{\tilde{p}_2} \frac{\partial\omega}{\partial p_2}\bigg|_{q_2=\tilde{q}_2} dp_2 ,$$

or

$$\begin{aligned}\omega(P) = \tau a\tilde{z} &+ \frac{1}{\alpha^3(\tilde{q}_1^2-1)} \int_{\lambda/\nu_3\alpha\tilde{q}_1}^{\tilde{p}_1} \frac{1}{(1-p_1^2)^2} \frac{\partial\psi_1}{\partial q_1}\bigg|_{q_1=\tilde{q}_1} dp_1 \\ &- \frac{1}{\alpha^3(\tilde{q}_2^2-1)} \int_{\lambda/\nu_3\alpha\tilde{q}_2}^{\tilde{p}_2} \frac{1}{(1-p_2^2)^2} \frac{\partial\psi_2}{\partial q_2}\bigg|_{q_2=\tilde{q}_2} dp_2 ,\end{aligned} \tag{4.6.11}$$

where relations (4.6.10) have been used. The integrals in equation (4.6.11) may be easily evaluated to give a series representation for the angle of twist (or angular displacement).

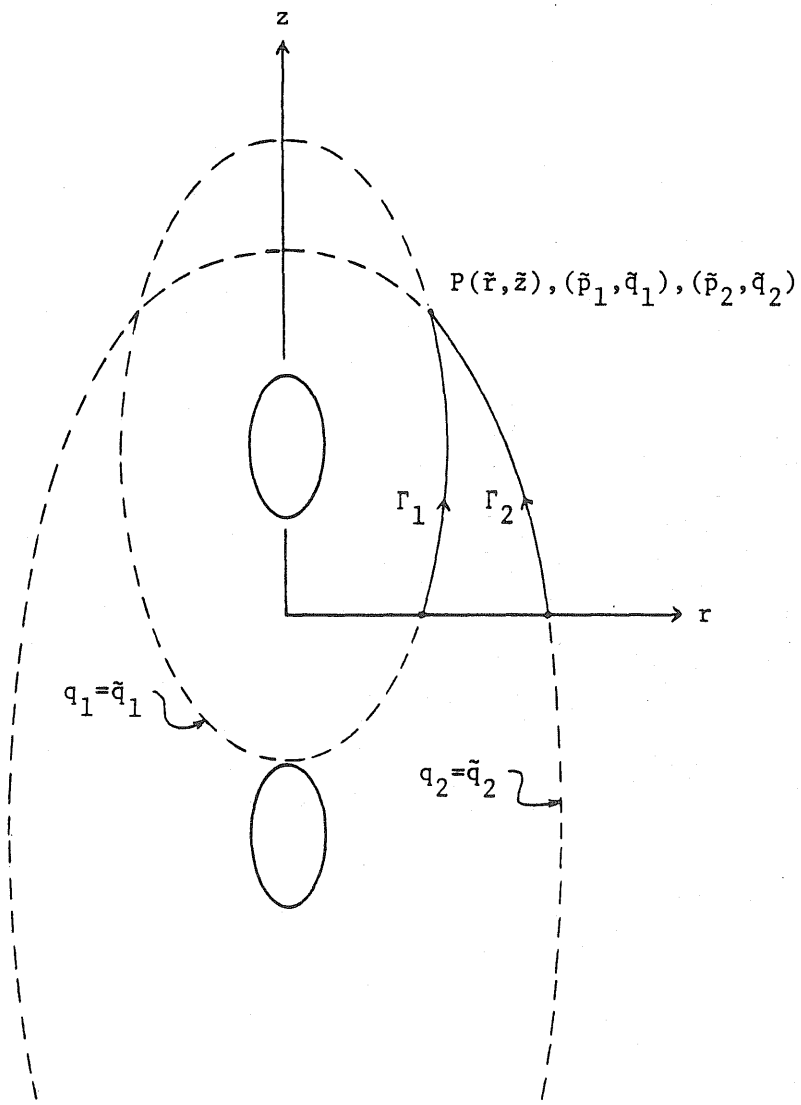

Fig. 4.6.1 Paths of Integration for ω

4.7 Stress Concentration and Stress Interference Factors

To examine the perturbing effect of the cavities, the stress concentration factor (SCF) is defined on the upper cavity surface as follows:

$$SCF = \frac{\sigma_{p\theta}^{(N)}(p)}{\sigma_{p\theta}^{(0)}(p)} \quad , \tag{4.7.1}$$

where

$$\sigma_{p\theta}^{(0)} = c_{44}\tau a \frac{\kappa(1-p^2)}{[\kappa^2-(\kappa^2-1)p^2]^{\frac{1}{2}}} \tag{4.7.2}$$

corresponds to the uniform field, and $p = \frac{z-\lambda}{\kappa}$ is the running variable on the upper cavity surface. Thus, the SCF is the ratio of the maximum shear stress at a point on the cavity surface to the corresponding stress component which would exist at that point if the body contained no cavities. Since both $\sigma_{p\theta}^{(0)}$ and $\sigma_{p\theta}^{(N)}$ vanish along the z-axis, the SCF assumes an indeterminate form for $p = \pm 1$. For these cases the appropriate limits must be taken. Using equations (4.6.4), (4.6.7), (4.7.1), and (4.7.2), and the asymptotic expressions [36]

$$\left.\begin{aligned} P_n^2(1-\varepsilon) &\sim \frac{(n+2)!}{4(n-2)!}\varepsilon \quad , \\ P_n^2(-1+\varepsilon) &\sim \frac{(-1)^n(n+2)!}{4(n-2)!}\varepsilon \quad , \end{aligned}\right\} \quad \text{as} \quad \varepsilon \to 0 \quad (\varepsilon > 0) \ ,$$

a lengthy computation will yield the SCF at the inner (p = -1) and outer (p = +1) poles of the cavity:

$$\lim_{p\to -1} \text{SCF} = 1 - \frac{q_0}{96\kappa^2} \sum_{n=2}^{N} A_n^{(N)} \frac{(-1)^n (n+2)!}{(n-2)!} \{ \frac{4\kappa^2}{q_0} [Q_n^2(q_0) + \frac{Q_n^2(q_2)}{\alpha^2(q_2^2-1)}] + \frac{1}{q_0^2-1} [(n-2)q_0 Q_n^2(q_0) - (n+2)Q_{n-1}^2(q_0)] - \frac{1}{\alpha^2(q_2^2-1)^2} [(n-2)q_2 Q_n^2(q_2) - (n+2)Q_{n-1}^2(q_2)]\} , \quad (4.7.3)$$

where $q_2 = (2\lambda - \kappa)q_0$;

$$\lim_{p\to +1} \text{SCF} = 1 - \frac{q_0}{96\kappa^2} \sum_{n=2}^{N} A_n^{(N)} \frac{(n+2)!}{(n-2)!} \{\alpha^2 \{ [\frac{4\kappa^2}{q_0\alpha^2} + (n-2)q_0] Q_n^2(q_0) - (n+2)Q_{n-1}^2(q_0)\} + \frac{(-1)^n}{\alpha^2(q_2^2-1)^2} \{ [\frac{4\kappa^2}{q_0} (q_2^2-1) + (n-2)q_2] Q_n^2(q_2) - (n+2)Q_{n-1}^2(q_2)\} \} , \quad (4.7.4)$$

where $q_2 = (2\lambda + \kappa)q_0$.

Again, since expressions (4.7.3) and (4.7.4) contain imaginary terms when $\kappa_3 < 1$, they are rewritten in terms of real quantities for computational purposes:

$$\lim_{p\to -1} SCF = 1 + \frac{\bar{q}_0}{96\kappa^2} \sum_{n=2}^{N} \bar{A}_n^{(N)} \frac{(n+2)!}{(n-2)!} \{ \frac{4\kappa^2}{\bar{q}_0} [\bar{Q}_n^2(\bar{q}_0) + \frac{\bar{Q}_n^2(\bar{q}_2)}{\bar{\alpha}^2(\bar{q}_2^2+1)}]$$

$$+ \frac{1}{\bar{q}_0^2+1} [(n-2)\bar{q}_0\bar{Q}_n^2(\bar{q}_0) + (n+2)\bar{Q}_{n-1}^2(\bar{q}_0)] \qquad (4.7.5)$$

$$- \frac{1}{\bar{\alpha}^2(\bar{q}_2^2+1)^2} [(n-2)\bar{q}_2\bar{Q}_n^2(\bar{q}_2) + (n+2)\bar{Q}_{n-1}^2(\bar{q}_2)]\} ,$$

where $\bar{q}_2 = (2\lambda - \kappa)\bar{q}_0$;

$$\lim_{p\to +1} SCF = 1 + \frac{\bar{q}_0}{96\kappa^2} \sum_{n=2}^{N} \bar{A}_n^{(N)} \frac{(n+2)!}{(n-2)!} \{ (-1)^n \bar{\alpha}^2 \{ [\frac{4\kappa^2}{\bar{q}_0\bar{\alpha}^2}$$

$$+ (n-2)\bar{q}_0]\bar{Q}_n^2(\bar{q}_0) + (n+2)\bar{Q}_{n-1}^2(\bar{q}_0)\}$$

$$+ \frac{1}{\bar{\alpha}^2(\bar{q}_2^2+1)^2} \{ \frac{4\kappa^2}{\bar{q}_0} (\bar{q}_2^2+1) + (n-2)\bar{q}_2]\bar{Q}_n^2(\bar{q}_2) \qquad (4.7.6)$$

$$+ (n+2)\bar{Q}_{n-1}^2(\bar{q}_2)\} \} ,$$

where $\bar{q}_2 = (2\lambda + \kappa)\bar{q}_0$.

In order to quantify the degree of stress interference between the two perturbing fields, the stress interference factor (SIF) is introduced:

$$SIF = \left[\frac{\sigma_{p\theta}\Big|_{\lambda\to\infty}^{(p)} - \sigma_{p\theta}(p)}{\sigma_{p\theta}\Big|_{\lambda\to\infty}^{(p)}} \right] \times 100\% \quad , \qquad (4.7.7)$$

where $\sigma_{p\theta}\big|_{\lambda\to\infty}$ corresponds to the single cavity solution which may be obtained by using the method of this chapter for a large value of λ (cavities far apart), or it may be derived from the stress function given by Bose [3]:

$$\psi\Big|_{\lambda\to\infty} = \psi_0 - \frac{\nu_3 \tau a}{12 Q_2^2(q_0)} \; r^2 \; P_2^2(p_1) \; Q_2^2(q_1) \; . \tag{4.7.8}$$

For the case of a spherical cavity this stress function generates boundary stresses of the form

$$\sigma_{p\theta}\Big|_{\lambda\to\infty}(p) = c_{44}\tau a \frac{2q_0}{(q_0^2-1)Q_2^2(q_0)} \; \frac{1-p^2}{q_0^2-p^2} \; .$$

From equation (4.7.7) it can be seen that the SIF represents the percent <u>decrease</u> in the maximum shear stress at a point on one of the cavity surfaces, due to the presence of the second cavity.

CHAPTER 5

NUMERICAL RESULTS AND DISCUSSION

5.1 General

In this chapter numerical results are presented for the case in which the two cavities are spherical, i.e., $\kappa = 1$. The variations of the stress concentration factor and the stress interference factor along a cavity surface are plotted for several values of ν_3 and λ. A summary of the recursion formula and series expansions involved in computing the associated Legendre functions $P_n^2(p)$ and $Q_n^2(q)$ (or $\bar{Q}_n^2(\bar{q})$) is given in the Appendix. Numerical procedures employed in the solution process included Legendre-Gaussian quadrature to obtain the coefficients $a_m^{(n)}$ (or $\bar{a}_m^{(n)}$) and Gauss-Seidel iteration for computing the superposition constants $A_n^{(N)}$ (or $\bar{A}_n^{(N)}$). A detailed discussion of these methods is given in [18]. Tables of roots and weights for Legendre-Gaussian quadrature are available in [11]. Ninety-sixth order quadrature was used in all computations and boundary stresses were calculated at the Gaussian points. Criteria for assessing the accuracy of the truncated solution are given in the present chapter, as well as a discussion of the numerical results.

5.2 Accuracy of Truncated Solution

In view of the rather complicated integral representations for $a_m^{(n)}$ and $\bar{a}_m^{(n)}$ (equations (4.2.9) and (4.3.4)), an analytic proof of convergence for systems (4.2.10) and (4.3.3) and their corresponding elastic states, as

$N \to \infty$, is difficult at best. However, based on physical considerations alone, it seems likely that the solution will converge for $\lambda > 1$. With this in mind, the value of N used in the computations was increased until the SCF (or $\sigma_{p\theta}^{(N)}$) became stabilized to the desired degree of accuracy. The values of N used were 30, 50, and 70. A second check on the accuracy is that the magnitude of the residual traction $|T_\theta^{(N)}(p)|$, or more importantly, the relative residual traction $\left|\frac{T_\theta^{(N)}(p)}{T_\theta^{(0)}(p)}\right|$, is "small". Here $T_\theta^{(0)}(p)$ is the traction on the cavity surface due to the uniform torsion field. For a spherical surface $T_\theta^{(0)}(p) = -c_{44}\tau ap(1-p^2)^{\frac{1}{2}}$. (In the vicinity of the equator it is required only that $|T_\theta^{(N)}|$ be small, since by its definition the relative residual traction possesses a singularity at $p = 0$.) Due to the nature of the problem, it seems reasonable that the relative residual should have a maximum near the inner pole. Indeed, for all computations performed, this conjecture was confirmed. Therefore, an indication of the degree of accuracy of each computed solution is given by the value of

$$\varepsilon(N; \lambda, \nu_3) \equiv \lim_{p \to -1} \left| \frac{T_\theta^{(N)}(p)}{T_\theta^{(0)}(p)} \right| , \tag{5.2.1}$$

the solution being more accurate for smaller values of ε. Using the second of equations (4.6.7), as well as equations (4.6.4), the limit in equation (5.2.1) may be evaluated to give the following explicit expressions for ε:

$$\varepsilon(N;\lambda,\nu_3) = \left|1 - \frac{1}{24}\sum_{n=2}^{N} A_n^{(N)} \frac{(-1)^n(n+2)!}{(n-2)!}\left\{Q_n^2(q_0) + \frac{Q_n^2((2\lambda-1)q_0)}{\alpha^2[(2\lambda-1)^2 q_0^2 - 1]}\right\}\right|,$$

$$\kappa_3 > 1; \qquad (5.2.2)$$

$$\varepsilon(N;\lambda,\nu_3) = \left|1 + \frac{1}{24}\sum_{n=2}^{N} \bar{A}_n^{(N)} \frac{(n+2)!}{(n-2)!}\left\{\bar{Q}_n^2(\bar{q}_0) + \frac{\bar{Q}_n^2((2\lambda-1)\bar{q}_0)}{\bar{\alpha}^2[(2\lambda-1)^2 \bar{q}_0^2 + 1]}\right\}\right|,$$

$$\kappa_3 < 1.$$

5.3 Variation of the Stress Concentration Factor

Figures 5.3.2 - 5.3.6 demonstrate the variation of the SCF along one of the cavities. Θ is the angle defined in Figure 5.3.1, and for the case of spherical cavities

$$p = \cos\Theta.$$

For $\lambda > 1$, the value of the relative residual traction was quite small for all computations, satisfying the following inequality:

$$\varepsilon < .00003.$$

In view of this small residual, as well as the observed stabilization of the SCF for increased N, the numerical results are believed to be accurate to at least the second decimal place for $\lambda > 1$.

For $\lambda = 1$ (contiguous cavities), accuracy to at least the second decimal place again appears to be obtained when $\nu_3 \geq 1$. For this range

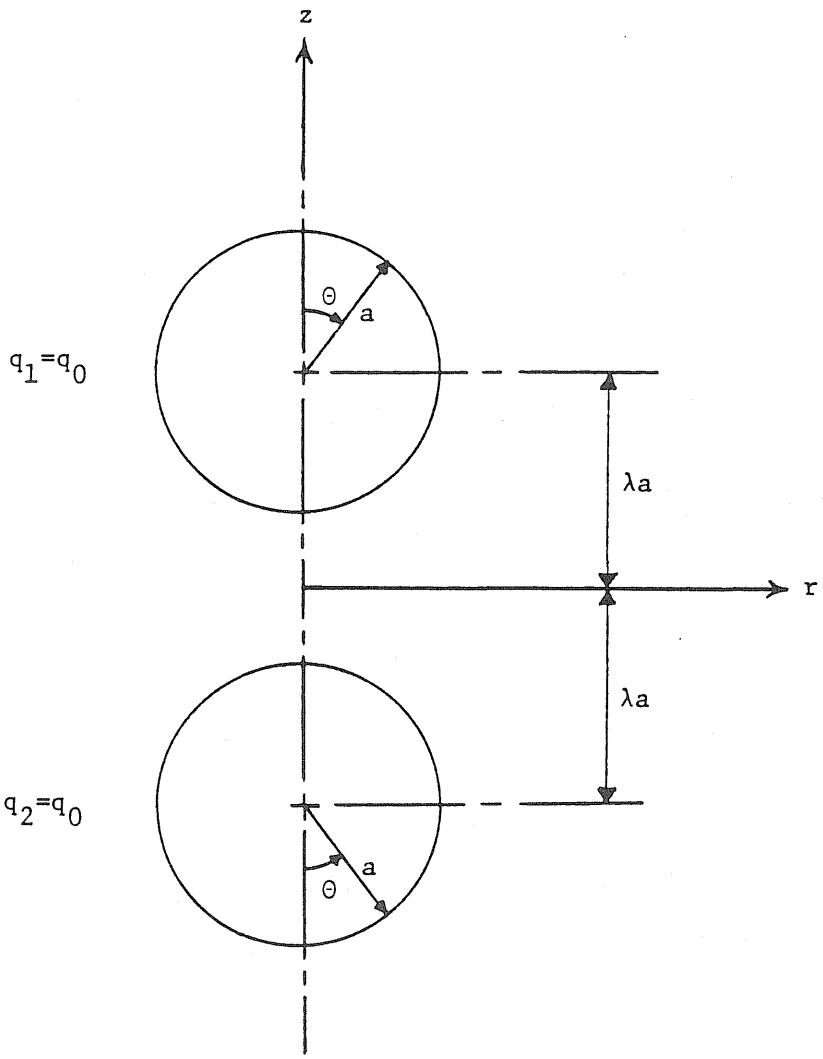

Fig. 5.3.1 Definition of Θ

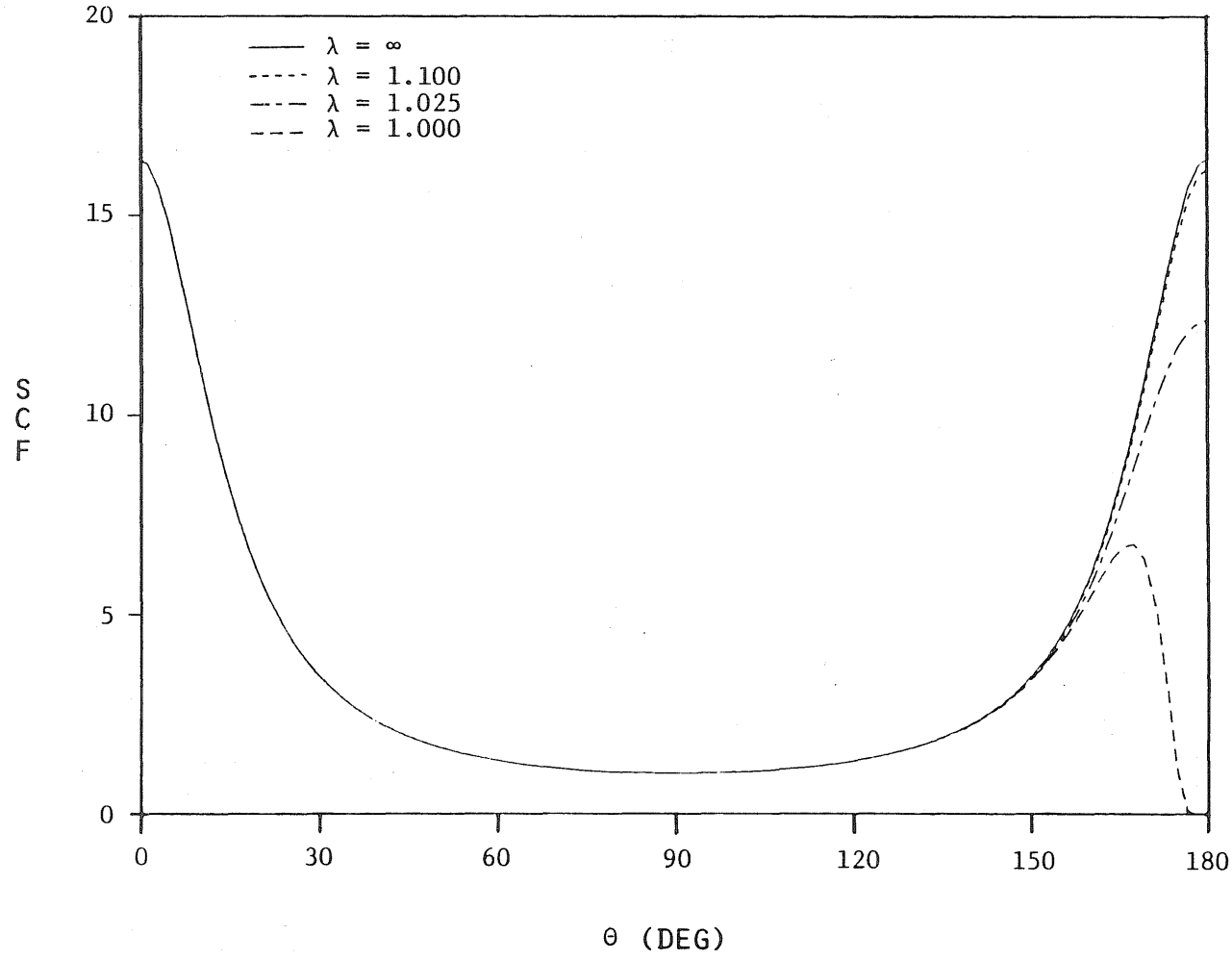

Fig. 5.3.2 SCF vs. Θ , ν_3 = 0.25

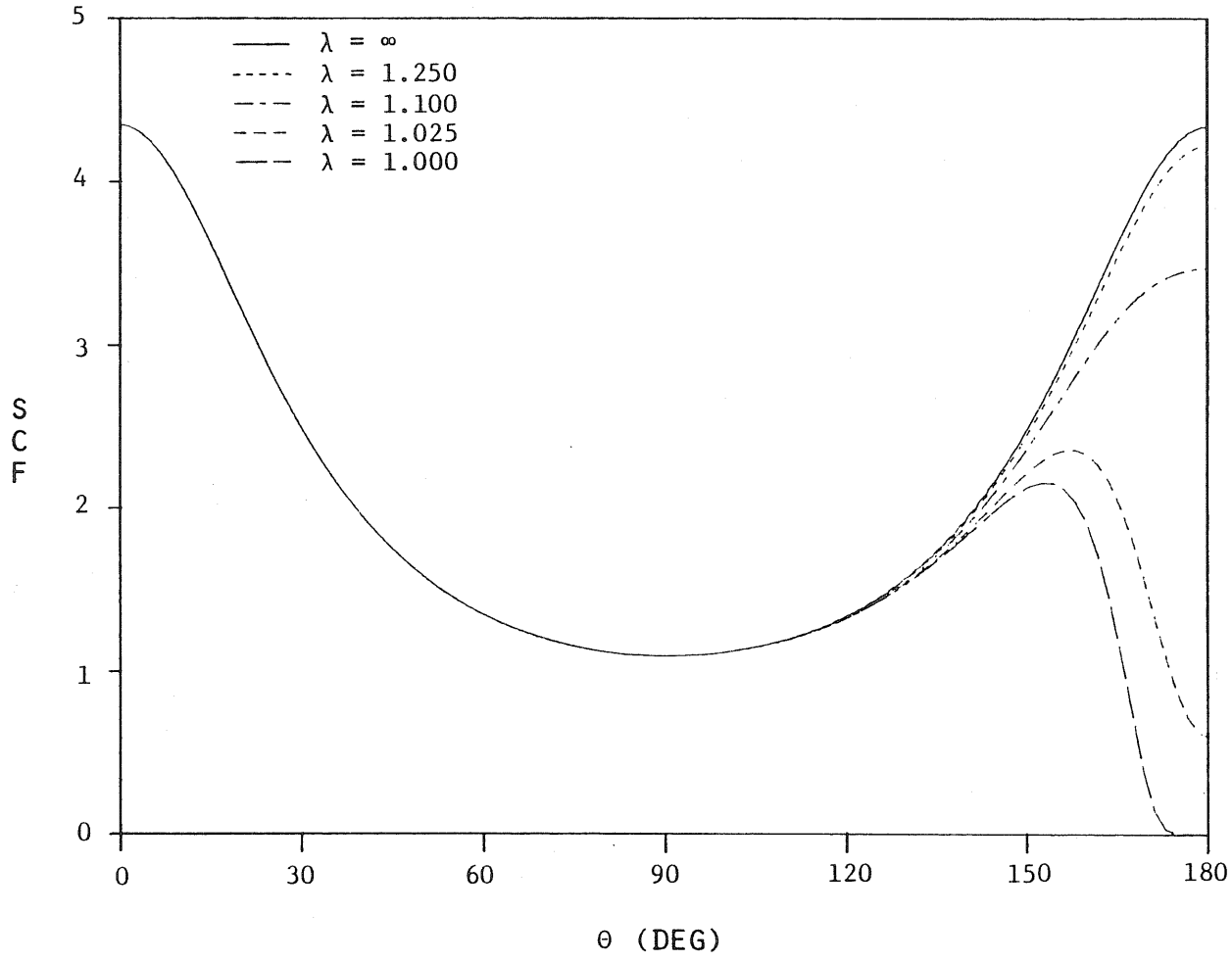

Fig. 5.3.3 SCF vs. Θ , ν_3 = 0.50

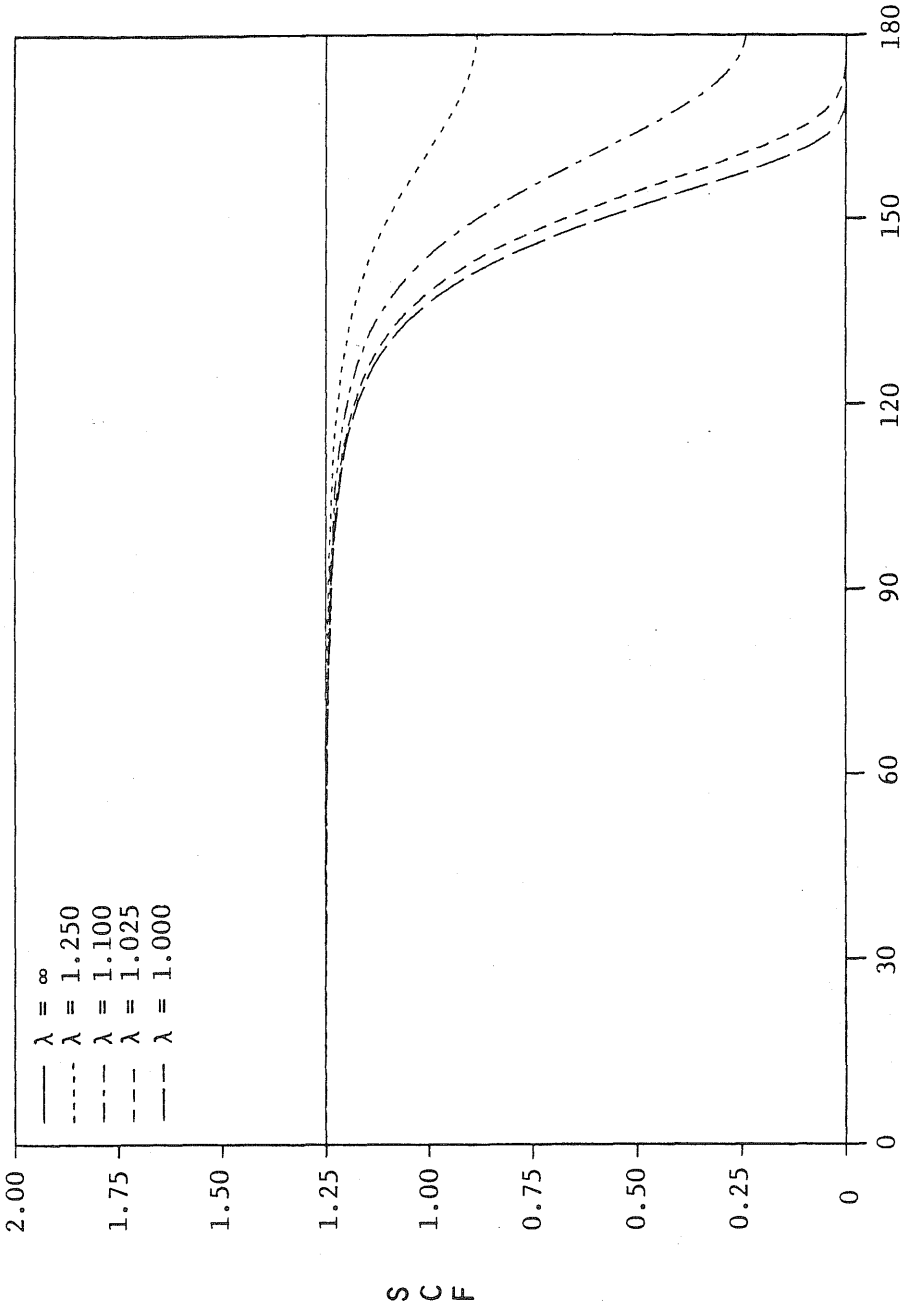

Fig. 5.3.4 SCF vs. θ , $\nu_3 = 1.00$

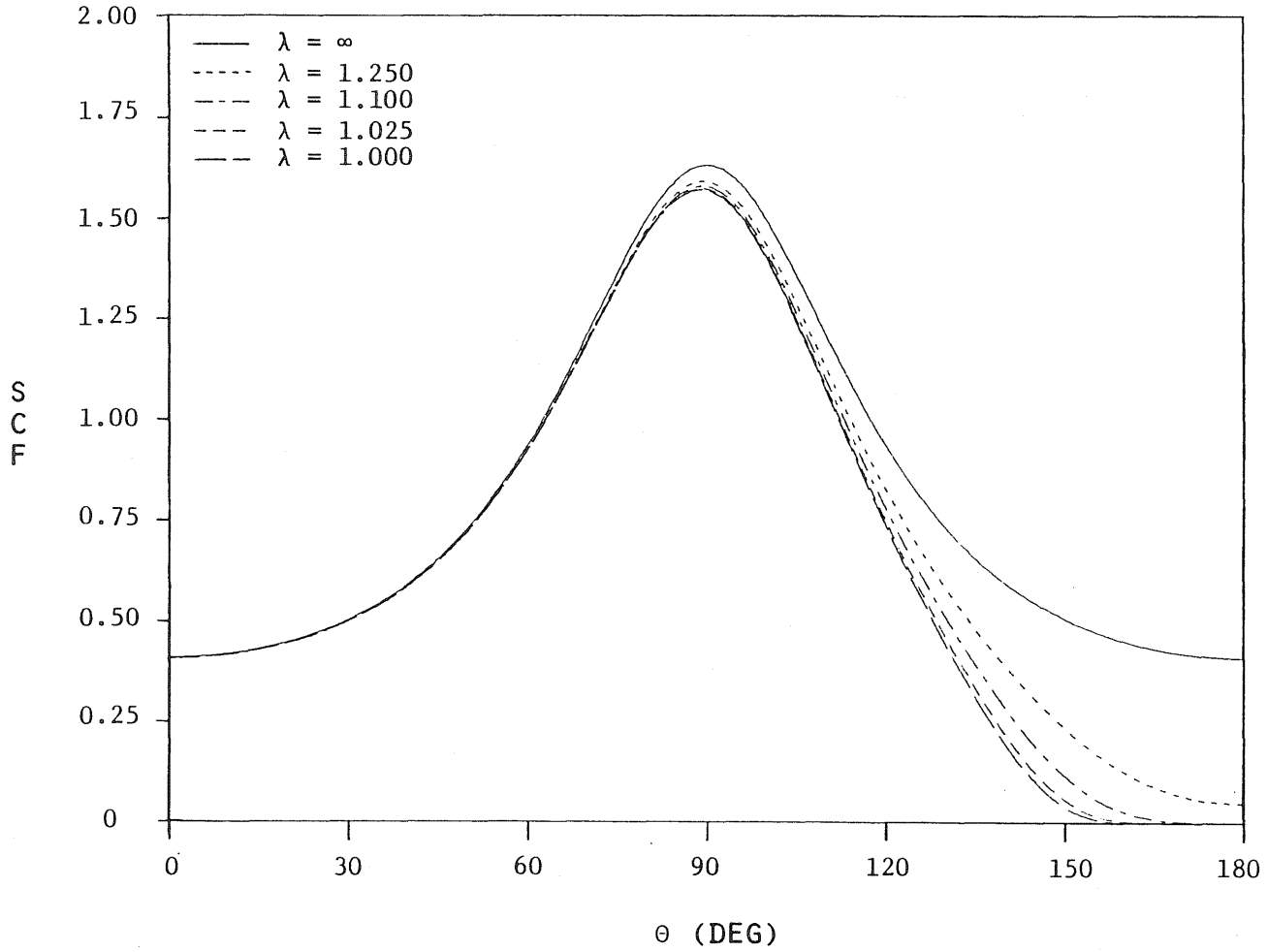

Fig. 5.3.5 SCF vs. Θ , ν_3 = 2.00

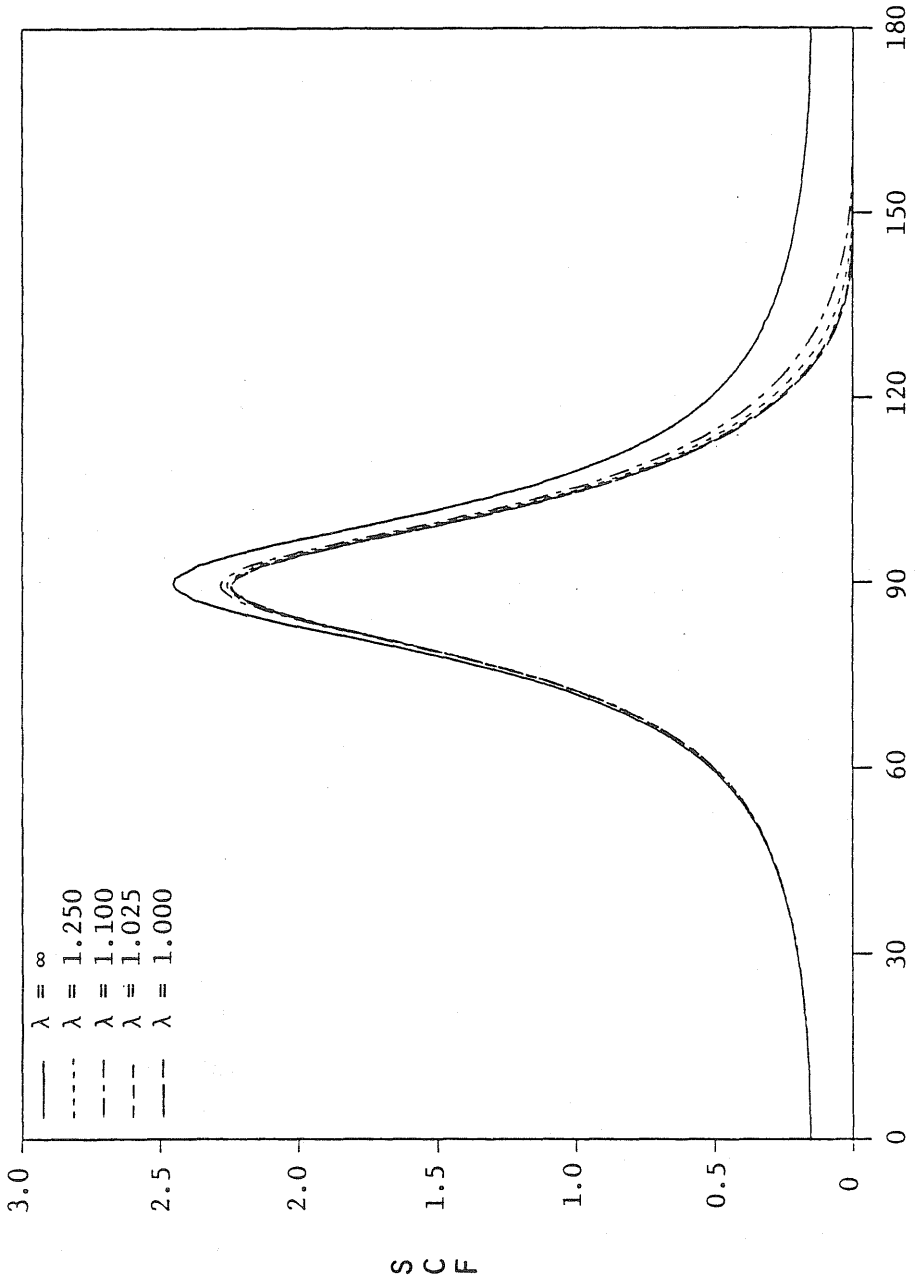

Fig. 5.3.6 SCF vs. θ , $\nu_3' = 4.00$

$$\varepsilon < .0001 \ ,$$

or, in other words, 99.99% of the uniform residual traction has been removed from the cavity. For the computations made for $\nu_3 < 1$, the following value was obtained:

$$\varepsilon = .004 \quad \text{for} \quad \nu_3 = .25, \ .50 \ .$$

The numerical results for these two values of ν_3 appeared to be stabilized only to the first decimal place in the vicinity of the inner pole, while for $\theta < 175°$ the values obtained are believed to be accurate to at least the second decimal place.

The following table summarizes the probable error bounds in the SCF values:

Table 5.1 Error Bounds in SCF Values

λ	ν_3	θ	Error
> 1	all	all	$\pm$ .005
1	≤ 1	all	$\pm$ .005
1	< 1	$< 175°$	$\pm$ .005
1	< 1	$175° \leq \theta \leq 180°$	$\pm$ .05

The $\pm$ .005 error bounds are adequate for the present purpose, while the slower convergence of the solution near the inner pole for $\lambda = 1$, $\nu_3 < 1$, is reason to consider reformulating the problem for this case in order to enhance convergence. This, however, is beyond the scope of the present study.

5.4 Variation of the Stress Interference Factor

In Figures 5.4.1 - 5.4.4 the SIF is plotted along one of the cavity surfaces for different values of λ and ν_3. These results are directly related to the SCF values, since equation (4.7.7) defining the SIF may alternately be written as

$$SIF = \left(\frac{SCF\big|_{\lambda\to\infty} - SCF}{SCF\big|_{\lambda\to\infty}} \right) \times 100\% \ .$$

The advantage of plotting the SIF instead of the SCF is that it gives a clearer picture of the interaction between the two perturbing fields. The numerical computations showed the SIF for all cases to be stabilized to within 0.5%

5.5 Discussion

From the SCF curves of Figures 5.3.2 - 5.3.6, it is seen that for each value of ν_3 all curves are bounded above by the curve corresponding to a single cavity ($\lambda \to \infty$). Therefore, all interference is destructive, in the sense that the two perturbing fields tend to cancel each other out. (This is also demonstrated in Figures 5.4.1 - 5.4.4, in which the percent interference is always positive.) Also, if the cavity spacing is decreased, the maximum shear stress at the cavity surface, $\sigma_{p\theta}$, becomes smaller.

The change in the general shape of the SCF envelope curves ($\lambda \to \infty$) as ν_3 varies is interesting to note:

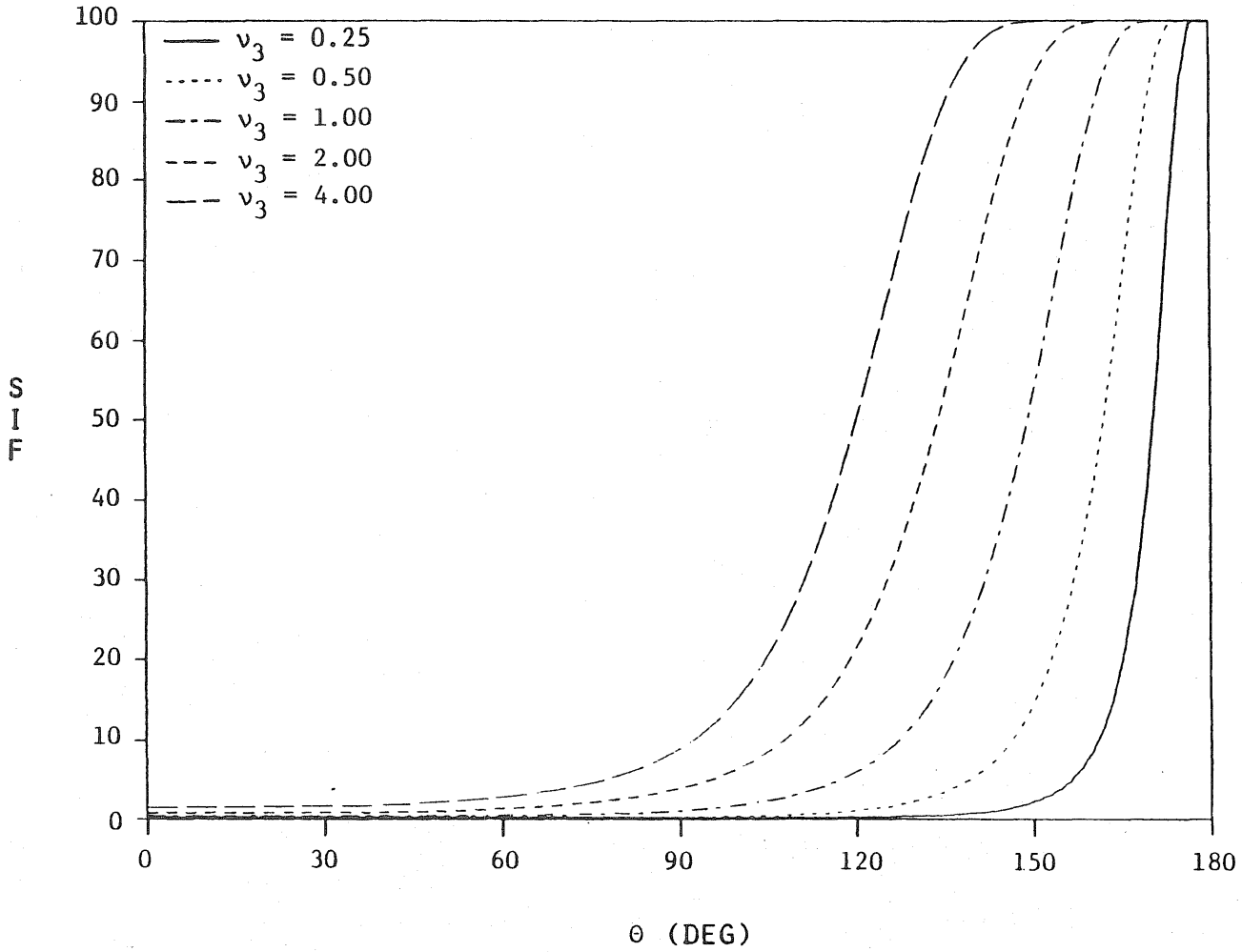

Fig. 5.4.1 SIF vs. Θ , λ = 1.000

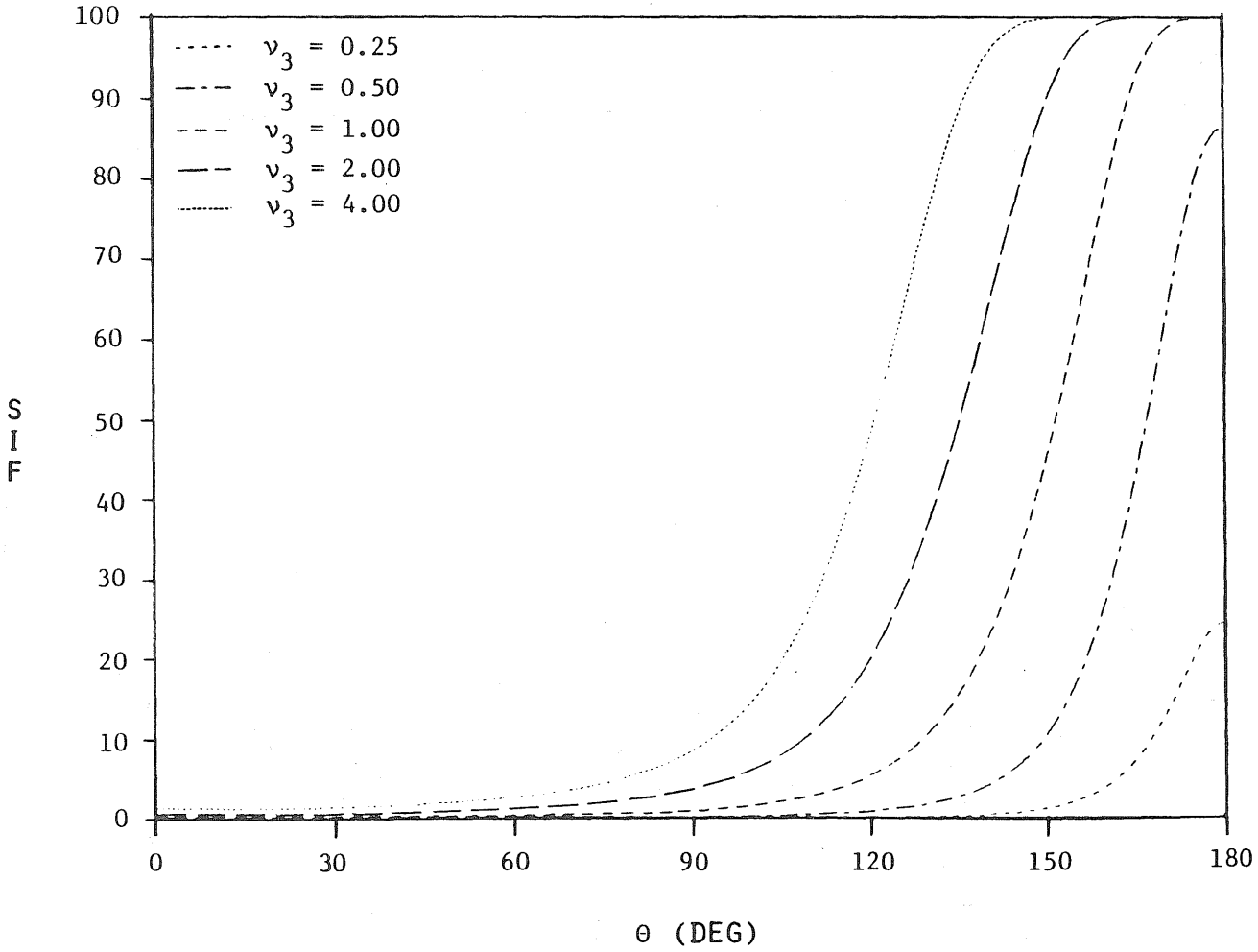

Fig. 5.4.2 SIF vs. θ , λ = 1.025

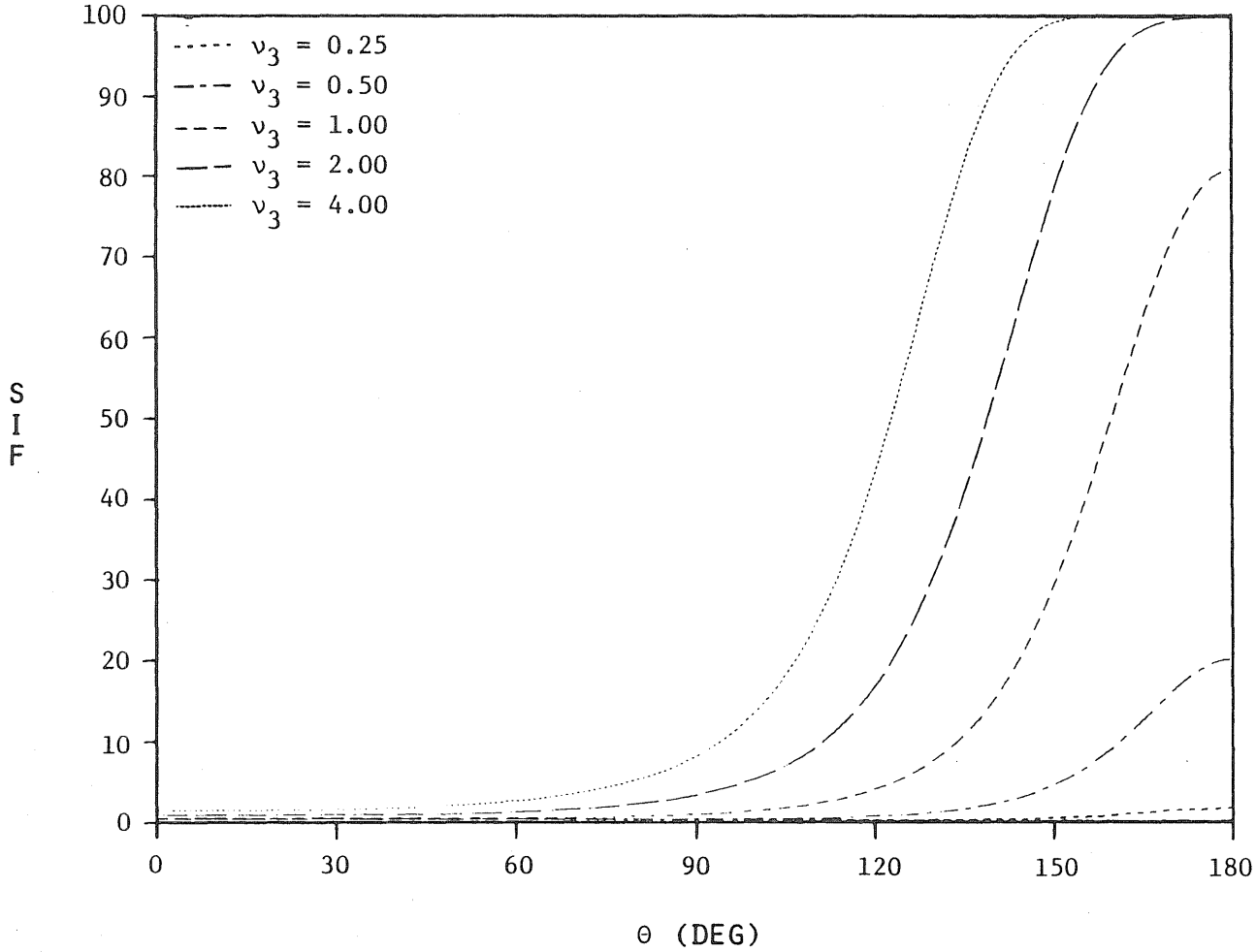

Fig. 5.4.3 SIF vs. θ , λ = 1.100

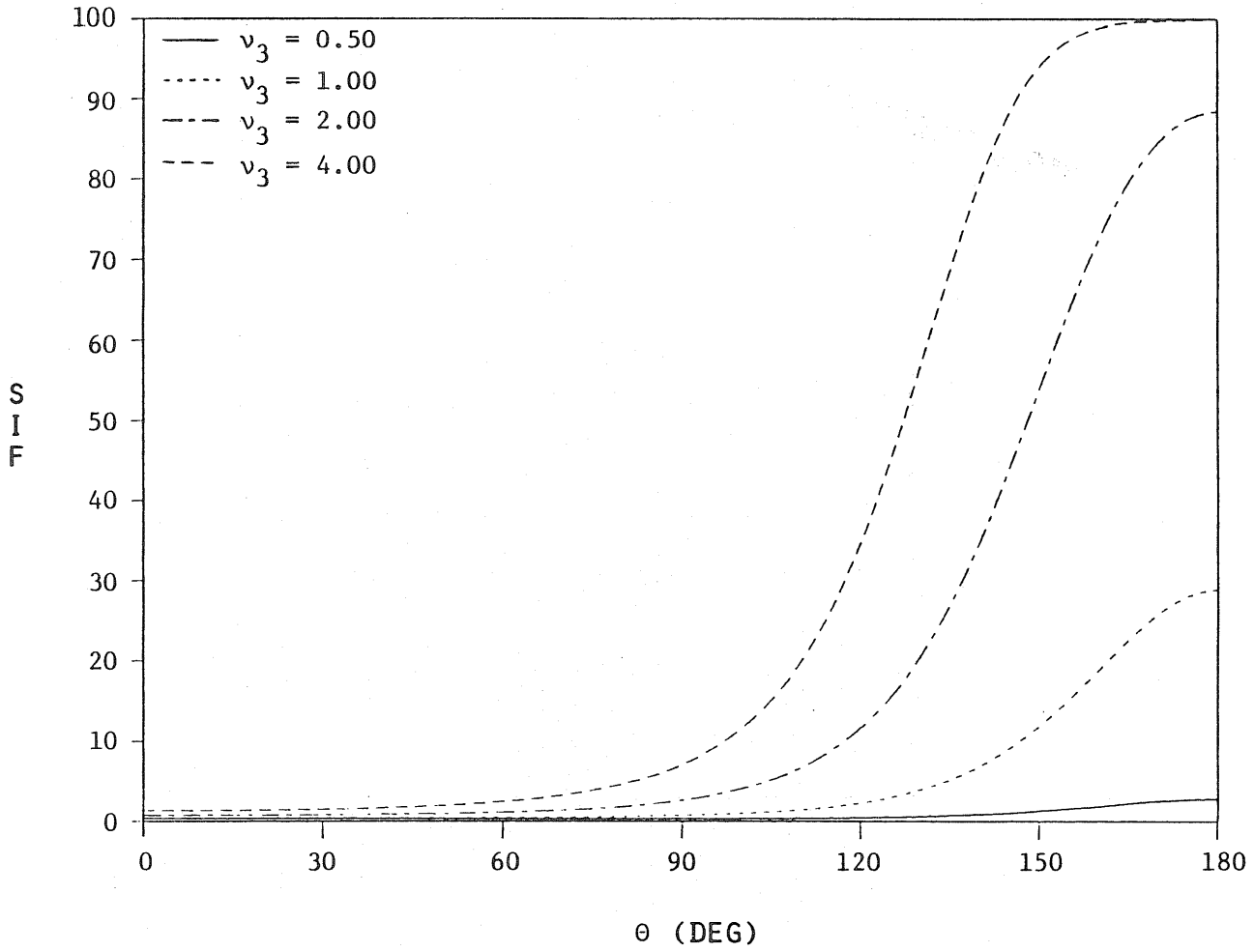

Fig. 5.4.4 SIF vs. Θ , λ = 1.250

1) For $\nu_3 < 1$, the maxima occur at the poles ($\theta = 0°, 180°$), the minimum at the equator ($\theta = 90°$).

2) For $\nu_3 = 1$, the envelope curve is constant.

3) For $\nu_3 > 1$, the maximum occurs at the equator, the minima at the poles.

Physically, this change in the nature of the curves may be explained by considering the equivalent isotropic problems (Section 2.2) corresponding to the various values of ν_3. The geometry for the isotropic problem is obtained by transforming the region occupied by the anisotropic body into the (r, θ, z_3)-space, i.e., by rescaling the z-axis. For $\nu_3 < 1$ the z-direction is "stretched" under this transformation, mapping the spherical cavities into prolate spheroids. For $\nu_3 > 1$ the z-direction is "shortened", resulting in a pair of oblate spheroidal cavities in the transformed space. In the limiting cases the following equivalent isotropic problems are encountered:

1) If $\nu_3 \to 0$, the cavities become needle-shaped cracks located along the z_3-axis.

2) If $\nu_3 \to \infty$, the cavities become penny-shaped cracks centered on and perpendicular to the z_3-axis.

For these two problems it is clear that the SCF will take on maximum values at the crack tips (points of maximum curvature) and minimum values at the points of minimum curvature. Thus for small ν_3 the peaks should be at the poles, while for large ν_3 the maximum SCF should occur at the equator. These qualitative conculsions are indeed confirmed by Figures 5.3.2 - 5.3.6.

The plots of the variation of the SIF show that as ν_3 increases, the interference becomes more pronounced. In other words the perturbations decay more slowly for the higher values of ν_3. For the idealized case of a unidirectional fiber-reinforced composite with inextensible fibers, ν_3 will approach infinity, and the perturbations will propagate throughout the medium in the z-direction. In terms of the equivalent isotropic problem, a large value of ν_3 effectively brings the transformed cavities closer together in the (r, θ, z_3)-space (their centers are separated by the distance $2\lambda_3 a = \frac{2\lambda a}{\nu_3}$), and it is therefore reasonable that the interference should increase as ν_3 increases. This is an indication that special care must be taken in applying Saint-Venant's principle to anisotropic media, as was noted by Horgan [22,23] for the two-dimensional case.

Another conclusion which may be drawn from Figures 5.4.1 - 5.4.4 is that, regardless of the cavity spacing, the interference is most pronounced in the range $90° < \theta \leq 180°$. For the range of ν_3 considered ($\nu_3 \leq 4$), in which most materials fall, the interference does not exceed 10% when $\theta \leq 90°$ (on the outer halves of the two cavities).

Since the SCF at the inner pole ($p = -1$) is most affected by the interference, some plots of $SCF\big|_{p=-1}$ or $SIF\big|_{p=-1}$ versus λ and ν_3 would provide insight into the phenomenon of stress interference. However, each point on each graph would require a separate computer run, thus prohibiting any detailed investigation of this type. Nevertheless, some interesting conclusions may be drawn from the few values of $SCF\big|_{p=-1}$ and $SIF\big|_{p=-1}$ given in the previous figures:

1) The SCF at the inner pole is relatively insensitive to λ for $\nu_3 > 1$. Its value ranges from 0 to 1.25 as λ varies from 1 to ∞.

On the other hand, for a fixed value of $\nu_3 < 1$, $SCF\big|_{p=-1}$ is quite sensitive to λ near $\lambda = 1$. For example, when $\nu_3 = .25$, the value of $SCF\big|_{p=-1}$ ranges from 0 at $\lambda = 1$ to 16.1 at $\lambda = 1.1$, but undergoes little additional change from the latter value as $\lambda \to \infty$. Thus, the relationship between $SCF\big|_{p=-1}$ and λ is highly nonlinear for $\nu_3 < 1$.

2) When $\lambda = 1$, the SCF at the inner pole appears to vanish for all ν_3.

3) For $\nu_3 \leq .5$ a spacing of $\lambda = 1.25$ yields less than 3% interference at the inner pole; i.e., the interaction is negligible. Therefore, the perturbations are extremely localized for small ν_3.

Conclusions concerning the SCF at the equator (p=0) include the following:

1) For $\nu_3 < 4$, the spacing of the cavities has little effect on $SCF\big|_{p=0}$.

2) The SCF at the equator for the single cavity solution is relatively insensitive to ν_3 -- it varies from 1 to 2.5 in the range of ν_3 considered.

3) As $\nu_3 \to 0$, $SCF\big|_{p=0} \to 1$ (corresponds to torsion of a hollow isotropic cylinder).

4) As $\nu_3 \to \infty$, $SCF\big|_{p=0} \to \infty$ (corresponds to torsion of an isotropic body with a penny-shaped crack).

The numerical results obtained include as special cases the following solutions:

1) the single cavity solution -- Bose [2] ($\lambda \to \infty$ in Figures 5.3.2 - 5.3.6)
2) the twin cavity solution for isotropy -- Eubanks [12] (Figure 5.3.4, $\nu_3 = 1$ in Figures 5.4.1 - 5.4.4)
3) the single cavity solution for isotropy -- Das [10] ($\lambda \to \infty$, $\nu_3 = 1$ in Figure 5.3.4).

CHAPTER 6

SUMMARY AND RECOMMENDATIONS FOR FURTHER STUDY

6.1 Summary of the Investigation

The torsion problem for a transversely isotropic body containing two spheroidal cavities has been solved and numerical results obtained for the case of two spherical cavities. The solution demonstrates the phenomenon of stress interference in a three-dimensional anisotropic elasticity problem. Viewing the problem as an equivalent isotropic problem with different geometry provides a convenient means of understanding the qualitative behavior of the stress concentration and stress interference factors. The results show that in all cases the presence of a second cavity tends to decrease the boundary stresses associated with the single cavity solution. Also, for fixed spacing, the degree of stress interference between the two cavities was shown to increase for increasing ν_3, implying that the perturbations damp out more slowly for larger values of ν_3. This should be an important consideration when applying Saint-Venant's principle to anisotropic problems.

6.2 Recommendations for Further Study

Some possible extensions of the present work are the following:

1) The present approach may be modified to solve the torsion problem of a transversely isotropic body containing two spheroidal inclusions. Rigid or elastic (isotropic or transversely isotropic) inclusions may be treated by altering the boundary conditions.

2) The method of solution may be generalized to consider more than two cavities or cavities of unequal size.

3) A modification of the present work may enable one to treat different loading cases -- pure shear, uniaxial and biaxial tension, and hydrostatic pressure. This would require a formulation in terms of two or three displacement potentials [24], as opposed to the single stress function in the case of torsion. As a result, one would need to introduce two or three spheroidal coordinate systems at each of the cavity centers, which coincide on the cavity surface. This would be an extension of the method employed by Chen [7-9] in solving the single cavity problem. The computation involved would obviously be more extensive, but the mathematical analysis should present no additional difficulties.

4) The method of solution employed for the torsion problem possessed an advantage over the method of spherical dipolar harmonics used for the isotropic analog [12], in the sense that it produced results which appeared to converge in the case of contiguous cavities. However, for $\nu_3 < 1$, this convergence was extremely slow in the vicinity of the inner poles, thus calling for a separate treatment in this case.

5) A more detailed numerical analysis of the present problem is needed to investigate the perturbation decay, not only in the longitudinal direction, but also radially. From a theoretical standpoint, it may be possible to extend the work of Knowles and Sternberg [28] on Saint-Venant's principle and the torsion of isotropic bodies of revolution to the transversely isotropic case.

APPENDIX

COMPUTATION OF THE ASSOCIATED LEGENDRE FUNCTIONS

A.1 Computation of $P_n^2(p)$

The associated Legendre function of the first kind, of degree n and order 2, is defined by

$$P_n^2(p) = (1-p^2)\frac{d^2}{dp^2}[P_n(p)] \quad , \quad -1 \leq p \leq 1 \quad ,$$

where the Legendre polynomial of degree n is given by [21]

$$P_n(p) = \frac{1}{2^n}\sum_{j=0}^{[\frac{n}{2}]}\frac{(-1)^j(2n-2j)!}{j!(n-j)!(n-2j)!}p^{n-2j} \quad ,$$

and the notation $[\frac{n}{2}]$ denotes the greatest integer less than or equal to $\frac{n}{2}$. Using equations (A.1.1) and (A.1.2) and performing some algebraic manipulation yields the following finite series for $P_n^2(p)$:

$$P_{2m}^2(p) = A(m)(1-p^2)\sum_{k=0}^{m-1}F_k(m)\,p^{2k} \quad ,$$

$$m=1,2,\ldots$$

$$P_{2m+1}^2(p) = B(m)(1-p^2)\sum_{k=0}^{m-1}G_k(m)\,p^{2k+1} \quad ,$$

where

$$A(1) = 3 \quad ,$$

$$A(m) = -\frac{2m+1}{2(m-1)} \; A(m-1) \quad , \quad m = 2,3, \ldots \quad ,$$

$$B(1) = 15 \quad ,$$

$$B(m) = -\frac{2m+3}{2(m-1)} \; B(m-1) \quad , \quad m = 2,3, \ldots \quad ,$$

$$F_0(m) = 1 \quad ,$$

$$F_k(m) = -\frac{(m-k)(2m+2k+1)}{k(2k-1)} \; F_{k-1}(m) \quad ,$$

$$G_0(m) = 1 \quad ,$$

$$G_k(m) = -\frac{(m-k)(2m+2k+3)}{k(2k+1)} \; G_{k-1}(m) \quad .$$

A.2 Computation of $Q_n^2(q)$

The two methods to be used in the computation of $Q_n^2(q)$, q real and $q > 1$, are the following:

1) Recurrence Relation,

2) Series Expansion.

Neither method alone is adequate for computing $Q_n^2(q)$ over the entire ranges of n and q needed. However, it can be shown that the following scheme of computation will guarantee a minimum of 12-digit accuracy in the value of $Q_n^2(q)$:

Table A.1 Computation Methods for $Q_n^2(q)$

q \ n	$2 \leq n \leq 10$	$11 \leq n \leq 50$	$51 \leq n \leq 70$
$1 < q \leq \frac{3}{2\sqrt{2}}$	Recurrence	Recurrence	Series*
$\frac{3}{2\sqrt{2}} < q \leq 3$	Recurrence	Series	Series
$3 < q < \infty$	Series	Series	Series

*Series is divergent but asymptotic for large n.

The two methods of computation will now be summarized. For a more detailed treatment of the subject, see the treatise by Hobson [21].

A.2.1 Recursion Formula for $Q_n^2(q)$

$$Q_1^2(q) = \frac{3}{q^2 - 1} \quad ,$$

$$Q_2^2(q) = \frac{3}{2}(q^2 - 1) \ln \frac{q+1}{q-1} - 3q + \frac{2q}{q^2 - 1} \quad ,$$

$$(n-2)Q_n^2(q) - (2n-1)q\, Q_{n-1}^2(q) + (n+1)Q_{n-2}^2(q) = 0 \quad , \quad n = 3,4, \ldots \ .$$

A.2.2 Series Expansion for $Q_n^2(q)$

Let $q = \cosh \xi$. Then $Q_n^2(q)$ may be represented by the series

$$Q_n^2(\cosh \xi) = C(n) \frac{e^{-(n+\frac{1}{2})\xi}}{\sinh^{\frac{1}{2}}\xi} \sum_{k=0}^{\infty} B_k(n) \left(\frac{1}{1 - e^{2\xi}}\right)^k , \qquad (A.2.2.1)$$

where

$$C(1) = 4\sqrt{2} ,$$

$$C(n) = \frac{2(n+1)}{2n+1} C(n-1) , \quad n = 2,3, \ldots ,$$

$$B_0(n) = 1 ,$$

$$B_k(n) = \frac{(2k+3)(2k-5)}{2k(2k+2n+1)} B_{k-1}(n) , \quad k = 1,2,3, \ldots .$$

The series in equation (A.2.2.1) is convergent for $q > \frac{3}{2\sqrt{2}}$, but is still useful when $1 < q \leq \frac{3}{2\sqrt{2}}$ and n is large. It can be shown [21] that the remainder after r terms is numerically less than the $(r+1)^{th}$ term, which approaches 0 as $n \to \infty$. Thus, the series is asymptotic for large n.

A.3 Computation of $\bar{Q}_n^2(\bar{q})$

The method of computing $\bar{Q}_n^2(\bar{q}) \equiv \frac{1}{i^{n+1}} Q_n^2(i\bar{q})$, $\bar{q}$ real and $\bar{q} > 0$, will be that of series expansion. Let

$$\bar{z} = \bar{q} + \sqrt{\bar{q}^2+1} \quad .$$

Then $\bar{Q}_n^2(\bar{q})$ may be represented by the series

$$\bar{Q}_n^2(\bar{q}) = D(n) \frac{\bar{q}^2+1}{\bar{z}^{n-2}(1+\bar{z}^2)^{5/2}} \sum_{k=0}^{\infty} B_k(n) \left(\frac{1}{1+\bar{z}^2}\right)^k \quad , \qquad \text{(A.3.1)}$$

where

$$D(1) = 32 \quad ,$$

$$D(n) = -\frac{2(n+2)}{2n+1} D(n-1) \quad , \quad n = 2,3, \ldots \ .$$

The $B_k(n)$ have been defined in Section A.2.2. The series in equation (A.3.1) is convergent for $\bar{q} > 0$. It can be shown that if the series is truncated after $k = m$, the truncation error E_m satisfies the following bounding condition:

$$E_m < \frac{1}{\bar{z}^2(1+\bar{z}^2)^m} \quad .$$

REFERENCES

1. Atsumi, A., "Stresses in a Circular Cylinder Having an Infinite Row of Spherical Cavities Under Tension," J. Appl. Mech., Vol. 27, pp. 87-92, 1960.

2. Bose, S. C., "On the Torsion of a Transversely Isotropic Circular Cylinder Having a Small Spherical Elastic Inclusion of an Isotropic Material," Zeitschrift fur Angewandte Mathematik und Mechanik, Vol. 45, pp. 133-135, 1965.

3. Bose, S. C., "Torsion of an Aeolotropic Cylinder Having a Spheroidal Inclusion on Its Axis," AIAA Journal, Vol. 3, pp. 1352-1354, 1965.

4. Chakravorty, J. G., "Concentrations of Stress in the Neighborhood of a Small Spherical Hole on the Axis of a Cylinder Under Torsion of Transversely Isotropic Material," J. of the Assoc. of Appl. Physicists, Vol. 4, pp. 13-20, 1957.

5. Chattarji, P. P., "Stress Concentrations Around a Small Spherical Inclusion on the Axis of a Transversely Isotropic Circular Cylinder Under Torsion," J. of the Assoc. of Appl. Physicists, Vol. 5, pp. 10-15, 1958.

6. Chen, W. T., "On a Spheroidal Elastic Inclusion in a Transversely Isotropic Material Under an Axisymmetric Torsion Field," J. Appl. Mech., Vol. 33, p. 944, 1966.

7. Chen, W. T., "Axisymmetric Stress Field Around Spheroidal Inclusions and Cavities in a Transversely Isotropic Material," J. Appl. Mech., Vol. 35, pp. 770-773, 1968.

8. Chen, W. T., "Stress Concentration Around Spheroidal Inclusions and Cavities in a Transversely Isotropic Material Under Pure Shear," J. Appl. Mech., Vol. 37, pp. 85-92, 1970.

9. Chen, W. T., "Elastic Analysis of an Axisymmetric Stress Field Perturbed by a Spheroidal Inhomogeneity," Quart. Appl. Math., pp. 517-525, 1971.

10. Das, S. C., "Stress Concentrations Around a Small Spherical or Spheroidal Inclusion on the Axis of a Circular Cylinder in Torsion," J. Appl. Mech., Vol. 21, pp. 83-87, 1954.

11. Davis, P. and Rabinowitz, P., "Additional Abscissas and Weights for Gaussian Quadratures of High Order: Values for n=64, 80, and 96," J. Research of the Natl. Bureau of Standards, Vol. 60, pp. 613-614, 1958.

12. Eubanks, R. A., "Stress Interference in Three-Dimensional Torsion," J. Appl. Mech., Vol. 32, pp. 21-25, 1965.

13. Eubanks, R. A. and Sternberg, E., "On the Axisymmetric Problem of Elasticity Theory for a Medium with Transverse Isotropy," J. Rat. Mech. Anal., Vol. 3, pp. 89-101, 1954.

14. Goree, J. G. and Wilson, H. B., "Axisymmetric Torsional Stresses in a Solid Containing Two Partially Bonded Rigid Spherical Inclusions," J. Appl. Mech., Vol. 34, pp. 313-320, 1967.

15. Greenberg, H., "An Engineering Basis for Establishing Radiographic Acceptance Standards for Porosity in Steel Weldments," J. Basic Engr., Vol. 87, pp. 887-893, 1965.

16. Gurtin, M. E. and Sternberg, E., "Theorems in Linear Elastostatics for Exterior Domains," Arch. Rat. Mech. Anal., Vol. 8, pp. 99-119, 1961.

17. Hashin, Z. and Rosen, B. W., "The Elastic Moduli of Fiber-Reinforced Materials," J. Appl. Mech., Vol. 31, pp. 223-232, 1964.

18. Hildebrand, F. B., Introduction to Numerical Analysis, Second Edition, McGraw-Hill, New York, 1974.

19. Hill, J. L., "The Effect of Two Rigid Spherical Inclusions on the Stresses in an Infinite Elastic Solid," J. Appl. Mech., Vol. 33, pp. 715-718, 1966.

20. Hill, J. L., "Pure Torsion of an Infinite Solid Containing Two Rigid Spherical Inclusions," J. Appl. Mech., Vol. 33, pp. 201-203, 1966.

21. Hobson, E. W., The Theory of Spherical and Ellipsoidal Harmonics, Macmillan, New York, 1931.

22. Horgan, C. O., "Some Remarks on Saint-Venant's Principle for Transversely Isotropic Composites," J. of Elasticity, Vol. 2, pp. 335-339, 1972.

23. Horgan, C. O., "On Saint-Venant's Principle in Plane Anisotropic Elasticity," J. of Elasticity, Vol. 2, pp. 169-180, 1972.

24. Hu, H.-C., "On the Three-Dimensional Problem of the Theory of Elasticity of a Transversely Isotropic Body," Acta Scientia Sinica, Vol. 2, pp. 145-151, 1953.

25. Huntington, H. B., The Elastic Constants of Crystals, Academic Press, New York, 1964.

26. Kirchhoff, G., "Über das Gleichgewicht und die Bewegung eines unendlich dünnen elastischen Stabes," J. Reine Angew. Math., Vol. 56, pp. 285-313, 1859.

27. Knops, R. J. and Payne, L. E., Uniqueness Theorems in Linear Elasticity, Springer-Verlag, New York, 1971.

28. Knowles, J. K. and Sternberg, E., "On Saint-Venant's Principle and the Torsion of Solids of Revolution," Arch. Rat. Mech. Anal., Vol. 22, pp. 100-120, 1966.

29. Kriz, R. D. and Stinchcomb, W. W., "Elastic Moduli of Transversely Isotropic Graphite Fibers and Their Composites," J. Experimental Mech., Vol. 19, pp. 41-49, 1979.

30. Lebedev, N. N., Special Functions and Their Applications, Dover Publications, Inc., 1972.

31. Lekhnitskii, S. G., Theory of Elasticity of an Anisotropic Body, Mir Publishers, Moscow, 1981.

32. Miyamoto, H., "On the Problem of the Theory of Elasticity for a Region Containing More than Two Spherical Cavities," Trans. of the Japan Soc. of Mech. Engrs., Vol. 23, pp. 431-436, 1957.

33. Moon, P. and Spencer, D. E., Field Theory Handbook, Second Edition, Springer-Verlag, New York, 1971.

34. Nisitani, H., "On the Tension of an Elastic Body Having an Infinite Row of Spheroidal Cavities," Trans. of the Japan Soc. of Mech. Engrs., Vol. 29, pp. 765-768, 1963.

35. Peterson, R. E., "The Interaction Effect of Neighboring Holes or Cavities, With Particular Reference to Pressure Vessels and Rocket Cases," J. Basic Engr., Vol. 87, pp. 879-884, 1965.

36. Robin, L., Fonctions Sphériques de Legendre et Fonctions Sphéroïdales, Tome I, II, and III, Gauthier-Villars, Paris, 1957.

37. Sokolnikoff, I. S., Mathematical Theory of Elasticity, Second Edition, McGraw-Hill, New York, 1956.

38. Shelley, J. F. and Yu, Y. Y., "The Effect of Two Rigid Spherical Inclusions on the Stresses in an Infinite Elastic Solid," J. Appl. Mech., Vol. 33, pp. 68-74, 1966.

39. Sternberg, E., "Three-Dimensional Stress Concentrations in the Theory of Elasticity," Appl. Mech. Reviews, Vol. 11, pp. 1-4, 1958.

40. Sternberg, E. and Sadowsky, M. A., "On the Axisymmetric Problem of the Theory of Elasticity for an Infinite Region Containing Two Spherical Cavities," J. Appl. Mech., Vol. 19, pp. 19-27, 1952.

41. Timoshenko, S. P. and Goodier, J. N., Theory of Elasticity, Third Edition, McGraw-Hill, New York, 1970.